1 **Customised fabrication of nitrogen-doped biochar for environmental and**

2 **energy applications**

3

4 Zhonghao Wan[1], Yuqing Sun[1], Daniel C.W. Tsang[1, *], Eakalak Khan[2], Alex C.K. Yip[3], Yun Hau

5 Ng[4], Jorg Rinklebe[5], Yong Sik Ok[6]

6 [1] Department of Civil and Environmental Engineering, The Hong Kong Polytechnic University, Hung Hom,

7 Kowloon, Hong Kong, China.

8 [2] Department of Civil and Environmental Engineering and Construction, University of Nevada, Las Vegas, NV

9 89154, USA.

10 [3] Energy and Environmental Catalysis Group, Department of Chemical and Process Engineering, University of

11 Canterbury, Christchurch, New Zealand.

12 [4] School of Energy and Environment, City University of Hong Kong, Kowloon, Hong Kong SAR, China.

13 [5] University of Wuppertal, School of Architecture and Civil Engineering, Laboratory of Soil- and Groundwater-

14 Management, Pauluskirchstraße 7, 42285, Wuppertal, Germany.

15 [6] Korea Biochar Research Centre, O-Jeong Eco-Resilience Institute (OJERI) & Division of Environmental

16 Science and Ecological Engineering, Korea University, Seoul 02841, Republic of Korea.

17

18 *Corresponding author email: dan.tsang@polyu.edu.hk

19

20   **Abstract**

21   Global warming, environmental pollution, and energy shortage are causing severe

22   environmental concerns worldwide. Conversion of various renewable biowastes into value-added

23   carbon-based material can be a promising option to alleviate these issues and ensure sustainable

24   development. The emergence of nitrogen (N)-doped biochar provides a versatile electroactive

25   platform suitable for environmental and energy applications. In this review, we summarise and

26   highlight the customised productions of N-doped biochars and their applications in environmental

27   remediation, energy storage, and biorefinery, *etc*. With a comprehensive overview on original

28   precursor, interspecies conversion, and ultimate deactivation of various N-dopants in biochar-

29   based carbocatalysis, their formation mechanism, distinct electrochemical characteristics, fate in

30   the environmental and energy applications, and electrochemical behaviours can be

31   comprehensively analysed. Contemporary challenges that require to be addressed, and

32   perspectives on improving N-doping technique on biochar are provided throughout the review.

33   Overall, this review can help to cultivate new insights in the customised production of N-doped

34   biochar for its broader applications in sustainable carbocatalysis and green chemistry.

35

36   **Keywords:** Engineered biochar; Nitrogen doping; Electroactive components; Advanced oxidation

37   processes; Green catalyst; Sustainable waste management.

38

1. Introduction

With the overwhelming progress of industrialization and modernization, ongoing anthropogenic activities are continuously proceeding to cater for enormous demands of growing human population for various aspects including energy supply, sustenance production, municipal administration, and so forth (Cha et al., 2016; Xiong et al., 2017). Accordingly, undesired biomass wastes will be inevitably generated as by-products or residues in these energy-consuming processes (Anastopoulos et al., 2019; Demirbaş, 2000; Li et al., 2016). Vast anthropogenic and refractory biowastes, *e.g.*, agricultural waste, forestry waste, animal manure, and municipal sewage sludge (Cho et al., 2019; Xu et al., 2019a), pose a potential threat to environmental ecosystems (*e.g.*, aquatic lives, atmospheric conditions, and soil contamination) as the annual generation of biomass has notably exceeded the natural degradation capacity. These waste streams carry financial costs for proper disposal and contribute to toxic leachate from landfills. In the past decades, conventional methods involving direct incineration, anaerobic composting, aerobic fermentation, and fodder production are extensively explored; however, these methods will either produce harmful greenhouse gases or require long operational time and spatial facilities, reluctantly constructing a healthy sustainable carbon recycle (Lee et al., 2017a).

To overcome the shortcomings above, several specific processing methods such as pyrolysis (Tripathi et al., 2016), gasification (Igalavithana et al., 2019; Yang et al., 2019a; You et al., 2017), and hydrothermal treatment (Gao et al., 2018; Wang and Wang, 2019) have drawn much attention due to their win-win merits. Particularly, pyrolysis under different operational parameters (*e.g.*, retention time, peak temperature, and ramping rate) can be applied to transform lignocellulosic biomass into desired biofuels (*i.e.*, syngas and tars) (Cho et al., 2017; Yang et al., 2019b). Meanwhile, the residual black carbon, namely biochar, can be simultaneously produced as a

62 permanent carbon sink to reach carbon sequestration, thus to mitigate the global warming induced

63 by carbon dioxide (CO_2) compared with the uncontrollable discharge from conventional disposal

64 (Palansooriya et al., 2019; You et al., 2017). It has been estimated that 0.1–0.3 billion tons of CO_2

65 can be deducted from the natural carbon cycle *via* biochar storage (Fowles, 2007). Furthermore,

66 the obtained biochar usually possesses well-developed porous structure and maneuverable surface

67 chemistry, which confer the potential to act as excellent adsorbent or catalyst in a wide array of

68 environmental applications (Bamdad et al., 2017; Kumar et al., 2020; Lee et al., 2017b). It has

69 been widely applied in environmental decontamination (Wan et al., 2019a; Wan et al., 2019b),

70 energy storage (Li et al., 2017), and soil amendment (Ahmad et al., 2014; Beckers et al., 2019; El-

71 Naggar et al., 2019), *etc*. Traditional carbonaceous materials produced from coal or petrochemical

72 products (*e.g.*, activated carbon (AC)), and the so-called "emerging" materials, such as carbon

73 nanotubes (CNTs) (Chen et al., 2018a), graphene oxides (GO) (Sun et al., 2012), and nanodiamond

74 (Lee et al., 2016), *etc*.) are fascinating at the research level. Yet, their applications in industrial

75 remain a challenge due to their complicated synthesis under harsh conditions with low yield. In

76 contrast, a more sensible and technologically viable approach is the creative utilization of biochar

77 produced from renewable and natural bioresource at a large scale (Igalavithana et al., 2019). The

78 emergence of biochar introduces a prospect alternative to facilitate green chemistry and sustainable

79 applications based on vast biomass.

80   Although raw biochar could be directly adopted as a versatile carbon substrate, the specific

81 surface area (SSA) and surface chemistry (*i.e.*, defective level and sp^2-hybridized carbon

82 framework) are limited due to the nonstoichiometric nature of original biomass (Duan et al., 2018).

83 Proper modification processes are usually required to tailor its properties for broader use.

84 Acid/alkaline treatment is commonly exploited as it could significantly promote SSA and surface

85   functionalization, providing more exposed active sites for further reactions (Cazetta et al., 2011;

86   Rajapaksha et al., 2016). Metal incorporation could significantly combine the advantages of

87   different transition metals (*i.e.*, ultrahigh reactivity, dense electron population, redox recycle, and

88   magnetism) and biochar framework (*i.e.*, porous structure, catalyst dispersion, and leaching

89   mitigation) (Cho et al., 2019; Yang et al., 2018; Yang et al., 2019c; Yi et al., 2020). Oxidizing or

90   reductive agents were deployed on biochar to tune the surface oxygen functionalities and SSA

91   (Wang et al., 2015a). Several activation techniques by changing purging gas from conventional

92   inert environment (*i.e.*, Ar or N_2) to reactive substrate (*i.e.*, steam or CO_2) were also introduced to

93   modify biochar structure (*i.e.*, micro- and mesopore evolution) (Igalavithana et al., 2019; Yang et

94   al., 2019d). Although these techniques have been extensively explored and showed great promise

95   in practical application; some irrevocable shortcomings hinder their footpath in green and

96   sustainable chemistry.

97   The controllable introduction of desired oxygen functionalities on biochar is still a tricky

98   challenge. Some types (*e.g.*, carboxylic group) can even exert negative influences to affect the

99   reducibility of biochar and cause an electron-deficient nature. In contrast, metal accommodation

100   prevails to circumvent this problem using oxygen functionalities as anchoring sites to stabilize

101   metal centres. Nevertheless, the introduced metal centres were generally reported to suffer from

102   unsolvable leaching and passivation, which might lead to secondary contamination irrespective of

103   their high efficiencies (Oh and Lim, 2019). Besides, the reversible regeneration of metal centres is

104   associated with high-temperature annealing with another stage of energy input. This inconvenient

105   regeneration process will increase the operational cost and thus impede practical application. To

106   sum up, a metal-free modification with low environmental concern is of considerable significance

107   to develop the sustainable nature of biochar.

108   The concept of metal-free heteroatom doping has been prevalent in carbonaceous communities

109   for several years (Ortiz-Medina et al., 2019). Doping technologies with earth-rich elements such

110   as nitrogen (N), boron (B), and sulphur (S), were exhaustively employed for synthesizing

111   nanocarbons. In general, it is well-acknowledged that the introduction of alien non-carbon atoms

112   into the ordered sp^2-hybridized carbon framework can alter the electrochemical capacities of the

113   original π-electron networks, creating an imbalanced electroactive state in the carbon structure to

114   deliver greater electrocatalysis (Frank et al., 2009; Yang et al., 2019e). The reactive sites can

115   promise stronger interactions with exterior molecules to achieve various purposes. It has been

116   reported that heteroatom doping technology, especially nitrogen doping (N-doping) with the

117   strongest efficacy, was applied to facilitate catalysis of nanocarbons, enhance detection limit of

118   sensors, and improve nanomaterial dispersion, *etc*.

119   From a chemical point of view, biochar produced under low-temperature treatment (< 700 ℃)

120   with a low graphitization degree is regarded as unsuitable for doping technology (Duan et al.,

121   2018). The graphitized biochar with a well-ordered and highly graphitized domain allowed the

122   heteroatom doping technologies to enter the field of biochar (Zhu et al., 2018). In recent years,

123   using biochar as fundamental carbon substrate to conduct N-doping to obtain high-performance

124   material has been tentatively explored. Most of the relevant studies on N-doped biochar clarified

125   that it remains a great challenge to explicitly elucidate the doping mechanism (Ding et al., 2020;

126   Ho et al., 2019). The physicochemical properties of biochar cannot be readily tuned due to the

127   inherent structural complexity of biochar and need further insights to construct a comprehensive

128   system. Besides, the origin of the catalytic mechanism is still vague and poorly stated as a result

129   of the disciplinary disparities. To unveil the underlying regularities might require exhaustive and

130   all-round understanding into the advances of carbon communities.

131   Several critical reviews with focal points on metal-free carbonaceous materials for

132   environmental and energy applications have been put forward (Duan et al., 2018; Li et al., 2018;

133   Liu and Dai, 2016; Miller et al., 2017). The concurrent stabilization of N and C utilizing suitable

134   biowastes shows fascinating preponderance over non-renewable nanocarbons to practically

135   mitigate environmental deterioration. However, these investigations neither addressed the

136   environmental sustainability of N-doped biochar nor interconnected the scalable synthetic

137   protocols with doping technologies to integrate disciplinary knowledge extended from mechanistic

138   chemistry to practical engineering. Systematic and comprehensive review to summarise the

139   integral progress of N-doped biochar in relevant practical applications is yet to be conducted. Thus,

140   it is indispensable to put forward this critical review to guide future research in fabrications, to

141   provide disciplinary insights on catalytic mechanisms, and to reach the wider application of this

142   high-efficient N-doped biochar ultimately.

143   Herein, this review will cover the following topics: (a) fundamental characteristics of N-doping

144   biochar and its typical N-dopants; (b) insights into the N-doping mechanism with an exhaustive

145   investigation on the fabrication procedures of N-doped biochar; and (c) applications of N-doped

146   biochar as adsorbent, electrocatalyst, and electrode material in different environmental fields. This

147   review will illustrate an integral fate of N-dopants on biochar in a sequential manner from the

148   original precursor, interspecies conversion, to ultimate attenuation/consumption. Furthermore, we

149   address different essential and technical challenges in each section from experimental and

150   mechanistic aspects, aiming to cultivate the customised and up-scaling production of N-doped

151   biochar in future environmental research.

152

153   **2. Formation and characteristics of different N species on biochar**

154   In principle, the incorporated nitrogenous contents mainly involve five types: (1) aminated

155   functionalities, (2) pyridinic N in six-membered heteroring, (3) pyrrolic N in five-membered

156   heteroring, (4) graphitic N (namely quaternary N or sp^2-hybridized nitrogen atom adjacent to three

157   sp^2-hybridized carbon atoms), and (5) oxynitrides ($-NO_x$) (Ortiz-Medina et al., 2019). The N-

158   dopants are likely to originate from the thermal cracking of initially attached aminated

159   functionalities. After the dehydration, condensation, and aromatization, the N atoms could be

160   successfully incorporated into carbon units at the expense of large fraction of volatile nitrogenous

161   contents.

162   Amongst, aminated functionalities (*i.e.*, primary, secondary, or tertiary amino) are functional

163   groups attached to the carbon surface under different pronated states. Typically, the alien N content

164   (*e.g.*, ammonia gas) will interact with the topological deviations of pristine graphitic carbon

165   network to grow along with the anchoring defective sites *via* covalent bonding interaction. The

166   generation of amino groups usually corresponds to the initial step to introduce N contents into a

167   carbon framework (Mian et al., 2019; Mian et al., 2018). With an electron-rich feature from

168   unpaired electrons, aminated groups can act as preferential adsorptive sites for reactant molecules

169   for better reactant-substrate contact. The aminated functionalities, however, are more susceptible

170   to the oxidizing environment (Wang and Wang, 2019) and, thus, give limited catalysis compared

171   with the doped N atoms (*i.e.*, pyridinic N, pyrrolic N, and graphitic N). Furthermore, the depletion

172   of electrons in the aminated groups after redox behaviours can readily generate oxynitride ($-NO_x$),

173   which is chemically inert for many catalytic reactions (Duan et al., 2015a).

174   Different from the surface aminated contents on biochar, N-dopant is more desired in redox

175   catalysis as it is prone to disrupt the electronic and spin features of biochar framework to improve

176   overall electrochemical capability rather than to donate electrons in a localized region. Pyridinic

177 N and pyrrolic N donate one and two p-electrons to the adjacent sp^2-hybridized carbon conjugated

178 framework to form p-type doping (Oh and Lim, 2019). Furthermore, edge-functionalized pyridinic

179 N and pyrrolic N with unpaired electrons are considered to donate electrons to participate in redox

180 reactions directly. The graphitic N inserted into an intact benzene ring is assigned to the sp^2-

181 hybridized N atom adjacent to three neighboring sp^2-hybridized carbon atoms. The n-type

182 graphitic N is generally regarded as the most conducive and electroactive N-dopant (Oh and Lim,

183 2019), which tends to interact with reactants to reduce their energy threshold to cleave/dissociate

184 respective chemical bonds. Compared with amino and oxynitride that maintain the fundamental

185 features of functional groups, the doped N atoms are energetically preferable to substitute the

186 carbon atoms at the edges of an ordered carbon unit to form heteroring at atomic scale (Gao et al.,

187 2019; Yang et al., 2019e).

188 With a higher electronegativity $vs.$ adjacent carbon atom (Pauling scale: $\chi_n = 3.04 > \chi_c = 2.55$),

189 the incorporation of these doped N atoms can induce a dipole moment, where the negatively

190 charged N atom as basic sites fulfill redox recycle and the positively charged adjacent carbon

191 atoms as the adsorptive sites intimately interact with exterior substances (Duan et al., 2015b; Sun

192 et al., 2014). The electron flow would follow a decoupled stage to restore the electrochemical state

193 of those N-dopants without irreversibly compromising the heteroatoms (Wan et al., 2020a).

194 Besides, the electron-deficient state of carbon atoms adjacent to doped N atoms is believed to

195 facilitate the overall reluctance of catalyst towards oxidative erosion, as the deactivation of biochar

196 mainly results from the carbon oxidation which impairs the reducibility, blocks the pore, and

197 changes the surface chemistry of carbon domain (Wu et al., 2020).

198 In summary, biochar engineered with controlled types and amounts of N-dopants could be

199 generated to meet the different practical demands of various environmental and energy

200   applications. Stoichiometric proportion of electroactive N-dopants and the customisation of their

201   yield and density in N-doped biochar need to be further elaborated. Due to the different thermal

202   stability of various N-dopants, the peak temperature is the critical factor that determines their yield

203   and diversity in the resultant catalysts, designated as essential operational parameters in **Table 1**.

204

205   **3.   Fabrication of N-doped biochar**

206   The N-doping techniques can be roughly categorised into two general types by different N

207   sources, *i.e.*, internal N source within biomass and external N source with additives or purging

208   ammonia. Based on the specific doping operation in practical fabrication, the doping style could

209   also be divided into *in-situ* doping on site and post-doping after carbonization. Their difference

210   consists in the participating timing of N source, where *in-situ* doping and post-doping are

211   correlated with the raw biomass and the already prepared biochar to be mixed with N source for

212   thermal treatment, respectively.

213   **3.1. N-doping with endogenous N contents in biomass**

214   The critical point for the self-doping of N into biochar relies on the selection of biomass. This

215   specified biomass should contain a large fraction of raw N contents within its overall chemical

216   components or inherent macromolecular structure. Biological substances like algae,

217   microorganisms, tissues, and other N-rich biowastes are more suitable to guarantee a high total N

218   level in resultant biochar.

219   For instance, Liang et al. (2018) chose water hyacinth, which is ubiquitous in eutrophic aquatic

220   ecosystems with outstanding N intake capacity, to produce a N-doped biochar cathode. The

221   biochar electrode was prepared by integrating 80 *wt.*% water hyacinth-derived biochar powder

222   (pyrolyzed at 800 ℃), 10 *wt.*% acetylene black, and 10 *wt.*% Polytetrafluoroethylene (PTFE) onto

223 titanium mesh under vacuum and dried at 100 ℃ for 2 h. The as-prepared N-doped biochar

224 electrode was claimed to possess ultrahigh N content (7.71 *at.*%) compared with those in other

225 reported biochars (2-7 *at.*%) (Shao et al., 2016). Accordingly, it exhibited excellent

226 electrochemical properties due to the introduced N-dopants, *i.e.*, pyridinic-N (43.2%) and

227 graphitic-N (56.8%). Another hydrophyte *agustifolia* was adopted by Ling et al. (2017) to produce

228 self-doped biochar at 600 ℃. The formed pyridinic N and pyrrolic N on biochar were found to

229 possess an unpaired electron with high reactivity.

230 Apart from the biological substances from aquatic ecosystems, banana peel was also adopted to

231 dope N into biochar by its endogenous N contents simultaneously. Specifically, Rong et al. (2019)

232 squeezed banana peels into a slurry state to reach homogeneity of raw feedstock. Then, a

233 hydrothermal treatment (180 ℃, 6 h) coupled with subsequent calcination (600 ℃, 2 h) was

234 sequentially proceeded to carbonize the feedstock. The contained N-dopants involved various

235 categories, *i.e.*, pyridinic N (28.5%), pyrrolic N (21.4%), and graphitic N (50.5%), due to the

236 relatively low thermal treating temperature, while only the pyridinic N and graphitic N were

237 proven effective in the catalytic activation.

238 Protein-rich biological substances are potentially suitable for the preparation of N-doped biochar.

239 Ho et al. (2019) fabricated a series of N-doped graphitic biochars from C-phycocyanin extracted

240 *Spirulina* residue, which is an N-rich cyanobacterium commonly applied in food science and

241 medicine industry. Peak temperatures, including 400, 700, and 900 ℃ were employed to tune the

242 types and density of N-dopants on biochar. An ultrahigh temperature over 900 ℃ was found to

243 effectively diminish unwanted N-dopants to reach higher graphitic N proportion (14.7%). The as-

244 prepared N-doped graphitic biochar exhibited higher graphitic degree and better conductivity,

245 which accounted for its superior catalysis in the environmental decontamination. Similarly, Ma et

246 al. (2019) employed human hair tissue as concomitant carbon and N sources to generate N-doped

247 biochar. The large fraction of incorporated pyrrolic N (58.5%) and graphitic N (41.5%) helped to

248 achieve a useful function in circulating electron flow inside the biochar matrix. Xie et al. (2020)

249 utilized a natural N-rich yeast (*Candida utilis*) to generate biochar nanosheets at 600 ℃. This work

250 abandoned the strategy to reach a highly graphitized carbon matrix and demonstrated that N-doped

251 biochar with a low graphitization degree also showed outstanding catalysis.

252   It is worth noting that the biochars derived from C-phycocyanin extracted *Spirulina* residue,

253 human hair, and *Candida utilis* all indicated a distinct non-radical activation of peroxides in

254 comparison to the conventional radical-dominated pathway (Liu et al., 2019a; Yu et al., 2019a).

255 This phenomenon was ascribed to the disrupted electronic feature of carbon framework owing to

256 the accommodation of abundant graphitic N. Besides, Yu et al. (2019a) employed municipal

257 sludge which was rich in N content due to the existence of endogenous polyacrylamide to fabricate

258 magnetic N-doped biochar under pyrolysis at 900 ℃. The self-doped N dopants, especially

259 pyridinic N (27.2%) and graphitic N (64.2%), contributed p-electrons to the graphitic carbon to

260 increase its catalytic capability (Luo et al., 2019; Oh et al., 2018).

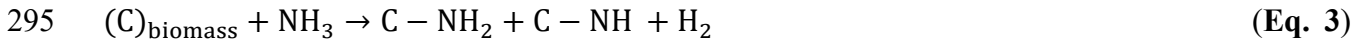261 **3.2. N-doping with external N precursors**

262   For the N-doping with exogenous nitrogen sources, the commonly adopted N additives

263 incorporate inorganic species (*e.g.*, ammonia, ammonium salts, and nitric acid) and organic species

264 (*e.g.*, urea, melamine, and aniline). In contrast to the endogenous N-doping, the addition or

265 impregnation of exterior N-rich substances target to construct an artificial nitrogenous ambient

266 environment (Lin et al., 2012; Wang et al., 2019a; Zhu et al., 2018). Thus, the operational

267 conditions might need to meet more strict and specific requirements. Upon the activation using

268 different N sources with distinct macromolecular structures and chemical compositions, the type

269 of the introduced N bonding configurations in resultant biochar also varied under various

270 operational conditions. It is worth noting that the abundance of oxygen-functional groups in

271 biomass demonstrates a positive correlation with the N-doping level in resultant biochar, as oxygen

272 functionalities can either directly bond with N precursor or undergo thermal decomposition to react

273 with N precursor (Duan et al., 2018).

3.2.1. Ammonia purging

275 Ammonia purging could provide NH_3 molecules to react with the carbon framework during

276 biomass thermal reforming, while their reaction intensity is relatively low and requires high-

277 temperature environment. Besides, the ammonia activation often occurs on the interfacial solid-

278 gas surface and leads to incomplete N-doping (*i.e.*, aminated contents) (Hou et al., 2019; Wu et al.,

279 2020). For instance, Mian et al. (2018) adopted NH_3 ambient pyrolysis to reach the transformation

280 of agar powder into N-rich biochar. The biochar precursor solids were pyrolyzed in a tubular

281 reactor with temperature progressively ramping to the desired peak temperature (800 °C) under Ar

282 environment (300 mL min^{-1}). Then, the Ar gas purging was promptly switched to ammonia

283 purging (28%, 500 mL min^{-1}) until the cooling-down stage. The possible formation mechanism of

284 attached N contents was then tentatively proposed, where the adequate −OH groups in agar powder

285 played the critical role by reacting with NH_3 molecules to produce amino groups (R−NH_2) at high

286 temperature (**Eq. 1**). The introduced amino groups further reacted with −OH to generate −C=N

287 (**Eq. 2**). Another possible pathway (**Eq. 3**) was described by Chen et al. (2016), as NH_3 was

288 regarded to react with carbonyl groups on biochar through Maillard reaction accompanied by H_2

289 production. Carboxyl groups were also considered to form hydrogen bonding with NH_3 to promote

290 N-doping and subsequently converted into pyridinic N and graphitic N (Jin et al., 2020).

291 Accordingly, ammonia purging was conducive to developing the microporous structure with the

292 consumption of oxygen functionalities (Yu et al., 2018).

293 $R - OH + NH_3 \rightarrow R - NH_2 + H_2O$ **(Eq. 1)**

294 $R - NH_2 + R - OH \rightarrow R - N = R + H_2O$ **(Eq. 2)**

295 $(C)_{biomass} + NH_3 \rightarrow C - NH_2 + C - NH + H_2$ **(Eq. 3)**

296 Similar preparation protocol was employed by Yu et al. (2018) and Lian et al. (2016) to produce

297 N-doped biochar derived from corn straw. The decoupled purging stages were exploited with three

298 sections at different holding temperatures, namely (a) N_2 ambient pyrolysis at 600 ℃ for 2 h for

299 biomass carbonization; (b) NH_3 ambient pyrolysis at 600 ℃ for 2 h to introduce N contents; and

300 (c) NH_3 ambient pyrolysis at 600, 700, and 800 ℃ for 1, 2, and 3 h to tailor the types and amounts

301 of N-dopants, respectively. The oxynitride was found to form at a lower peak temperature and a

302 shorter holding time (600 and 700 ℃ for 1 h), further confirming that the activation reaction

303 initiated from the reaction between oxygen functionalities and NH_3 molecules. Pyridinic N or

304 pyrrolic N was transformed into graphitic N with the increase of peak temperature and retention

305 time, indicating the feasibility of tailoring N-dopants by controlling operational conditions. The

306 illustrative doping process is depicted in **Fig. 1**. As shown in **Table 1**, a high temperature over

307 800 ℃ is more suitable to consolidate N atoms into biochar framework. Overall, the plausible

308 formation of graphitic N by ammonia purging was initiated at the surface functionalities through

309 the sequential transformation of pyrrolic N to pyridinic N, and finally to the terminal graphitic N.

310 **3.2.2. Ammonium salts**

311 Zhu et al. (2018) fabricated N-doped graphitic biochar using a wetland plant (reed) as biochar

312 precursor and ammonium nitrate (NH_4NO_3) as N source. As indicated in **Fig. 2a**, the pulverized

313 reed powder was immersed and agitated in 50 mL ethanol containing 1 g ammonium nitrate to

314 achieve the homogenous dispersion of N source over biomass. After implementing the solvent

315   evaporation at 85 °C, the obtained mixed slurry was annealed at 900 °C to produce N-doped

316   biochar with high graphitic N ratio (61.7 *at.*% of the total N content). The employed ammonium

317   salt seemed to act as both a pore-forming structural modifier and a reductive N-doping agent

318   because it simultaneously releases NH_3, N_2, or N_2O during the thermal decomposition. A similar

319   conclusion was proposed by Zhou et al. (2018) in the preparation of N-doped biochar using N-

320   containing phosphates. The added salts mainly decomposed into NH_3 modify the carbon surface

321   during pyrolysis. It can be assumed that the mechanistic formation route of N-dopants using

322   ammonium salts is similar to that using ammonia purging, whereby the NH_3 molecules first

323   combine with defective sites terminated with oxygen functionalities and subsequently are

324   converted to respective N-dopants.

325   **3.2.3. Organic additives**

326   N-doping using organic additive is a handy one-pot method to obtain N-doped biochar, as it only

327   requires the homogenous mixing of biomass and organic additive. The subsequent preparation

328   procedure can follow that of conventional biochar production, which makes it more accessible for

329   scientific communities.

330   Amongst all organic nitrogen additives, urea is a ubiquitous representative as it contains both

331   carbon and N elements, which is conducive to the introduction of alien N atoms into carbon matrix

332   *via* co-polymerization of biomass and N source. As shown in **Fig. S1a**, Oh et al. (2018) adopted

333   lignocellulosic spent coffee grounds mixed with urea to fabricate N-doped biochar. The

334   preparation procedure consisted of simple mixing by agate mortar and subsequent direct pyrolysis,

335   and the weight ratio of biomass to urea and peak temperature was set at 1:5 and 1000 °C,

336   respectively. This simple procedure avoided the complicated gas purging and post-treatments to

337   remove salt depositions. Impregnation of urea on biomass is another available approach to reach

338   homogeneity of feedstocks. Ding et al. (2020) immersed 2 g rice straw into 80 mL water containing

339   0.75 g dissolved urea. After solvent evaporation, the mixed slurry was transferred to a tubular

340   reactor for pyrolysis at 1000 °C. The weight ratio between biomass and N source was 2:0.75.

341   Compared with dry mixing, the impregnation can reduce the N source dosage irrespective of an

342   additional solvent evaporation process.

343   The N-doped biochar related to urea activation generally reported the ultrahigh SSA due to the

344   decomposition of urea within the biomass. This phenomenon might result from the thermal

345   instability of mixed urea to release NH_3 to open up pores. Wang et al. (2019b) however claimed

346   the radicals might be formed during the decomposition of urea at high temperatures and corrode

347   biomass to reach a richer porosity. Chen et al. (2019) considered urea might act as an expansion-

348   reduction agent to cause more reduction and exfoliation during the preparation of reduced GO,

349   which coincided with the phenomenon reported in N-doped biochar fabrication.

350   For operational conditions using organic additives, the reaction temperature should be carefully

351   controlled as the N-rich sources such as urea and melamine tend to decompose into different

352   intermediate products under specified peak temperature. Oh et al. (2018) claimed that the urea

353   would undergo polycondensation to generate intermediate products including cyanuric acid and

354   melamine. Carbon nitride would be formed during the initial pyrolytic stage at 300 °C with the

355   appearance of various aminated moieties (*i.e.*, $-NH_2$, N$-$H, and C$-$N) on biochar surface. When

356   the temperature was elevated to above 400 °C, these N-based moieties could be decomposed and

357   coalesced into carbonized biomass lattice to form various N-doped bonding configurations (*i.e.*,

358   pyridinic N, pyrolytic N, and graphitic N). As temperature further increased to above 700 °C, only

359   a large fraction of graphitic N could be preserved. Besides, urea could not diffuse into biomass

360   internal macrostructure (Zaeni et al., 2020), suggesting that preliminary controlling the particle

361   size of the feedstock may favour introduction of more N contents.

362   Similarly, melamine decomposition also follows decoupled stages with different intermediates.

363   An inert product, such as C_3N_4, would be primarily generated in a lower pyrolytic temperature (<

364   600 °C), and only a minor amount of melamine could be incorporated to form N-dopants (Wang

365   et al., 2019c). A higher temperature over 700 °C could help to consolidate N-dopants and to

366   develop a graphitic lattice. Although most organic additives require different temperatures to

367   decompose, the type of N-dopants tends to follow a distinctive order with 700−800 °C as the

368   borderline (as shown in **Table 1**), *i.e.*, pyridinic N and pyrrolic N dominate when peak temperature

369   is lower than 700 °C and graphitic N governs at a higher temperature over 800 °C. Holding time

370   marginally influences the compositions of N bonding configurations, which is different from

371   ammonia purging or ammonium salts activation (Oh et al., 2018). This suggests that the organic

372   additives would coalesce N atoms into carbon lattice *via* co-polymerization, different from the

373   carbon surface interaction with NH_3 molecules.

374   **3.3.Co-doping technologies**

375   Although sole doping of sulphur (S), boron (B), phosphorus (P), or iodine (I) into carbon matrix

376   was reported to be ineffective for carbon-based catalysis (Duan et al., 2015c), tailoring the

377   physicochemical properties of N-doped biochar by co-doping another foreign atom into a carbon

378   matrix is triggering attention, as this technique might increase the reactivity of N-doped biochar

379   by introducing synergistic bonding configurations. Due to the different electrochemical properties

380   of each alien atoms in terms of their atomic radius and orbitals, electronegativities, and electron

381   density, the electronic and spin nature of N-doped biochar could be further tailored.

382   As shown in **Fig. 3a-d**, Ma et al. (2019) found the slight co-doping of S contents (1.04 *at.*%) in

383   the N-doped biochar derived from human hair notably enhanced its electrochemical carbocatalysis.

384　The doped sulphur contents mainly consisted of thiophene S on the edge sites rather than inert

385　oxygenated S. Considering the close electronegativity between carbon and S atoms (Pauling scale:

386　$\chi_s = 2.58$ *vs.* $\chi_c = 2.55$), the coalesced S atoms might cause a distinct spin-dominated activation to

387　reach a spin disruption in comparison to the charge-dominated regime from sole N activation

388　(Ortiz-Medina et al., 2019). The positive role of S to synergize with doped N atoms in the

389　carbocatalysis was also reported on other carbonaceous materials like graphene (Duan et al., 2015d;

390　Liang et al., 2012). Nevertheless, Ding et al. (2020) claimed the S doping negatively influenced

391　the catalytic capacities of N-doped biochar, indicating that the co-doping technique on biochar is

392　still in its embryonic stage and need further elucidation.

393　　Boron is another earth-abundant element applied in the heteroatoms doping technique. Chen et

394　al. (2019) successfully doped N and B on a simplified carbon platform, *i.e.*, graphene, to

395　manufacture a highly efficient catalyst. The substituted B atoms in graphitic carbon structure were

396　capable of promoting graphitization degree and suppressing oxidative corrosion. The bonding

397　configurations among C, N, and B were vital to determine the reactivity of resultant composite, as

398　B can easily neutralize the unpaired electron of N-dopants to cause an electron-deficient region

399　(Zhao et al., 2013). The B-C-N heteroring was considered to be most reactive, especially when B

400　atoms were in the meta position of N atoms. In contrast, hexagonal boron nitride appeared to be

401　chemically inert and inhibited carbocatalysis (Ma et al., 2011). No relevant biochar research

402　reported the co-doping of N and B, which might result from that inherent complexity and vague

403　interpretation.

404　　Apart from non-carbon heteroatoms doping, metal atoms with dense electron population were

405　also involved in this co-doping scheme. Different from conventional metal incorporation, the co-

406　doped metal atoms need to maintain the metallic state by Me-N-C or Me-O-C bonding

407   configurations to give rise to the electrochemical state in the interactive region. Zhong et al. (2020)

408   successfully fabricated N-Cu co-doped biochar, and the Cu atoms were auto-reduced by biomass

409   when calcinated under the inert gas environment. However, it remains inconclusive whether metal

410   could be regarded as heteroatoms irrespective of their high electroactive efficacy.

411   **3.4. Emerging fabrication methods**

412   Apart from traditional pyrolysis, several emerging processing methods have been developed to

413   produce N-doped biochar. Hydrothermal carbonization process can be conducted at a relatively

414   low temperature (*i.e.*, 160–300 ºC) and an autogenic high pressure (*i.e.*, 200–600 bar). During the

415   ionic reaction between biomass and water-induced ions (*i.e.*, hydronium and hydroxide ions) under

416   subcritical conditions (Sevilla and Fuertes, 2009), the addition of N-containing contents might lead

417   to the successful doping. Nevertheless, the primary dopants derived from hydrothermal

418   carbonization are barely elaborated at the present stage. Besides, a thermochemical microwave

419   method was also applied to enhance the N-doping, and the main dopant was found to be pyridinic

420   N (12.9–15.7%), pyrrolic N (45.6–58.3%), and graphitic N (28.7–38.6%) (Wang et al., 2018a).

421   Wan et al. (2020b) also found that microwave-assisting ammonia purging led to the primary edge-

422   nitrogenation of pyridinic N (11.5%) and pyrrolic N (42.9%) on cellulose-derived biochar. The

423   mechanochemical ball-milling process was adopted to introduce nitrogenous contents onto biochar

424   (Xu et al., 2019b). The kinetic energy of moving balls potentially broke the inert carbon structure

425   and incorporated a certain amount of N functionalities. At the same time, the energy appeared too

426   weak to convert surface nitrogenous functionalities into N-dopants. Non-thermal atmospheric

427   plasma with low energy input was found to induce a spontaneous N-doping during biochar

428   fabrication, although the types and densities of nitrogen dopants remained unclear (Mbouopda et

429   al., 2018; Tiya-Djowe et al., 2019). Overall, these techniques can significantly reduce the energy

430   input, which might trigger new strategies for facile N-doping. The relevant research is still scarce

431   and can be further complemented.

432   **3.5. Limitations of different N-doping methods**

433   Under different practical purposes, the specified operational procedure could be selected to

434   reach the desired N-dopants for the expected demand. Compared with post-doping treatment, the

435   *in-situ* doping is more effective in incorporating N into carbon lattice, because N source can

436   experience the integral carbon reforming processes during the biomass pyrolysis, *i.e.*, dehydration,

437   decarboxylation, condensation, repolymerization, and aromatization (Sun et al., 2014).

438   Accordingly, the occurrence of N content to be coalesced into re-united hexagonal rings is

439   facilitated. In contrast, the already prepared biochar, especially the highly graphitized ones

440   prepared under high temperature (> 700 °C), is well-ordered and tends to demonstrate inert and

441   stable features resisting alien atom doping. As a consequence, the N-doping style for those under

442   the post-doping procedure is generally limited to the edge-nitrogenated types (*i.e.*, pyrrolic N and

443   pyridinic N) bound onto biochar surface.

444   Apparently, the self-doping technique avoids the addition of toxic or costly chemicals (Gao et

445   al., 2016). It tightly matches with the sustainable and green feature of biochar production without

446   the involvement of extra energy or chemical inputs. Thus, its practical significance is

447   recommended to be highlighted in future work. Considering that the N contents are well-

448   acknowledged to be thermally unstable until combined into intact hexagonal carbon units, the

449   endogenous self-doping is energetically preferential to fix nitrogen contents and mitigate their

450   release into the atmosphere. Furthermore, the biomass wastes requiring disposal are abundantly

451   available worldwide and vary in chemical compositions. More attention should be paid on the

452   selection of proper biomass and its low-cost transformation into heteroatoms self-doped catalysts

453   in the future.

454   To assure more introduced N-dopants, a continuous ammonia purging flow or a tightly sealed

455   reactor is usually a necessity, which significantly increases the operational difficulties and impedes

456   the up-scaling application. The employment of inorganic N sources can cause a deposition of

457   inorganic salts to form a monolayer dispersed on the surface of resultant biochar (Ho et al., 2019;

458   Xu et al., 2020). The interaction between biomass and impregnated N-containing substances is

459   usually a single-layer process that preferentially takes place on the carbon surface, leading to a

460   reduced SSA and a blocked porous structure. Post-treatment methods such as pickling or acid

461   washing are available to alleviate this issue. However, this complicated preparation procedure is

462   not practically and economically attractive. Thus, the N-doping using ammonium salts is

463   recommended to coordinate with other techniques that require similar post-treatment such as

464   molten salt activation (*e.g.,* $ZnCl_2$) to reach simultaneous surface cleaning.

465   N-doping using organic additives seems to be facile, economical, and controllable compared

466   with the aforementioned methods. The resultant N-dopants can also be tuned under different peak

467   temperatures to meet specified practical demand. Nevertheless, the adoption of organic sources

468   such as urea will ineluctably release greenhouse gas (*i.e.*, NO_x) due to the incomplete combustion

469   of feedstocks. This would exert long-term detrimental global effects from the life cycle perspective.

470   In the future study, the optimization between practical significance and environmental concern is

471   recommended to be further analyzed.

472

473   **4.   N-doped biochar for different applications**

474   With the tuned chemical properties (*e.g.*, surface chemistry, graphitization degree, and defective

475   level) and structural properties (*e.g.*, SSA, porosity, and morphology) owing to the introduced N-

476 dopants, N-doped biochar with superior capability has been applied in various fields mainly

477 involving adsorption, catalytic remediation, and energy conversion and storage.

4.1. Adsorption of pollutants

479 Adsorption is a conventional process to reach phase separation of pollutants from its original

480 medium to remediate environmental contamination in air, soil, or aqueous solution. Biochar

481 adsorption mechanisms for organic pollutants mainly involves electrostatic force, hydrogen

482 bonding, pore-filling adsorption/partition, π–π interaction, and hydrophobic interaction (Sun et al.,

483 2019), while its adsorptive performance towards metal/metalloids is governed by ion exchange,

484 cation–π bonding, metal-ligand complexation with surface oxygen functionalities, and co-

485 precipitation with endogenous mineral contents (Sun et al., 2020; Zhong et al., 2019a).

486 It is generally known that the adsorption capability of biochar is highly correlated with the type

487 of precursor feedstock. For instance, biochar prepared from biowastes with high ash contents (*e.g.*,

488 animal manure and sewage sludge) are more efficient in removing metal/metalloids due to the high

489 cation exchangeability, but inert towards organics. Overall, the adsorption efficiency of raw

490 biochar is still limited without further physical/chemical modification. The scientific community

491 is, therefore, particularly interested in fabricating biochar that could target a broad spectrum of

492 pollutants to increase its practical applications. The emergence of N-doping is regarded as a

493 potential game-changer, as it can introduce N-dopants to improve both the basicity of carbon

494 surface to facilitate the electrostatic interaction and the textural characteristics of biochar to

495 provide more interactive region.

4.1.1. Adsorption of metals and metalloids

497 Metals and metalloids usually undergo interspecies conversion when ambient pH changes. Thus,

498 the electroactive contents on the interfacial carbon surface play a vital role in the removal of metals

499   and metalloids. The introduction of various N-dopants, known as typical basic sites, could readily

500   provide unpaired electrons to accommodate metal cations onto biochar surface. As indicated in

501   **Table 3**, the best adsorption performance of various N-doped biochars was found to take place

502   below neutral pH values, because the protonation of introduced N-dopants in the acidic

503   environment could help to attract more metal cations. As shown in **Fig. S2**, an agar derived biochar

504   activated by NH_3 (ABF-N_{800}) achieved a high Cr(VI) adsorption capacity of 142.9 mg g^{-1} *via*

505   enhanced electrostatic interaction attributed to the introduced nitrogenous contents (Mian et al.,

506   2018).

507   N-dopants can also enhance the hydrophilicity of the biochar surface to facilitate the contact

508   with metal ions in solution and coordinate with metals and metalloids to form a chemical

509   complexation. Yu et al. (2018) reported the excellent adsorption performance of N-doped biochar

510   derived from crop straw towards both Cu(II) (1.63 mmol g^{-1}) and Cd(II) (1.76 mmol g^{-1}), and the

511   adsorptive mechanism was mainly ascribed to surface complexation with graphitic N and surface

512   hydroxyl groups. Ling et al. (2017) fabricated N-doped biochar derived from hydrophyte to

513   stabilize Pb(II) with an ultrahigh removal efficiency of 893 mg g^{-1}, and the surface coordination

514   by pyridinic N, pyrolytic N, and C=O was regarded as the adsorptive mechanism.

515   Biochar produced *via* hydrothermal carbonization with a higher surface electron population was

516   also reported to exhibit favourable affinity towards heavy metals. Guo et al. (2019) investigated

517   the effect of peak temperature on the adsorption capacities and selectivity of *Camellia sinensis*

518   derived N-doped biochar. Biochar produced at 240 °C (HTC-240) was found to show the highest

519   adsorption performance toward Cu(II), Pb(II), and Cr(VI) with adsorption capacities at 44.0, 83.9,

520   and 94.7 mg g^{-1}, respectively. High-temperature biochar (HTC-280) exhibited a higher adsorption

521   affinity towards Zn(II) with an adsorption capacity of 64.8 mg g^{-1}. Despite the chemical

522 complexation, several other mechanisms involving mass transfer, intraparticle diffusion, and

523 chemisorption also participated due to the modified extrinsic properties during N-doping.

524 Similarly, Gai et al. (2016) utilized endogenous N contents in a microalgae (*Chlorella pyrenoidosa*)

525 to modify rice husk-derived biochar *via* hydrothermal carbonization. The prepared N-doped

526 biochar showed an increased Cu(II) adsorption capacity to 29.1 mg g^{-1} compared with 13.1 mg g^{-}

527 ^{1} of raw biochar. The adsorption mechanism was governed by surface complexation rather than

528 electrostatic attraction.

4.1.2. Adsorption of organics

530 Compared with metals and metalloids, organics are more nucleophilic due to their electron-rich

531 macromolecular compositions. Accordingly, the evolved π–π electron donor-acceptor interaction

532 and Lewis acid-base interaction by N-dopants on N-doped biochar dictate the adsorption of organic

533 pollutants. Besides, the introduction of N-dopants can cause electron redistribution by polarizing

534 π electron from carbon layers and create positive holes, which may show a strong affinity with

535 electron-rich aromatic rings (Wang et al., 2018a). As illustrated in **Fig. S3**, Yang et al. (2017)

536 fabricated a wheat straw derived N-doped biochar sheet for atrazine removal. The adsorption

537 capacity reached 82.8 mg g^{-1}, and the principal mechanism originated from π–π electron donor-

538 acceptor interaction between atrazine molecules and electron-deficient carbon region. Li et al.

539 (2019a) synthesized a corn stalk derived N-doped biochar and reached enhanced phenol adsorption

540 ability at 95.9 mg g^{-1}. Both Lewis acid-base interaction and electron donor-acceptor interaction

541 contributed to the removal of phenol. These interactions were also considered to account for the

542 removal of dyes, *i.e.*, acid orange 7 and methyl blue with removal capacities of 292 and 436 mg g^{-}

543 ^{1}, respectively, by corn straw derived N-doped biochar (Lian et al., 2016). Lu et al. reported (2017)

544 the increased basicity of N-doped biochar could enhance its affinity towards acidic pollutants

545 (bisphenol A, 9.68 mg g^{-1}).

546   Besides, N-doped biochar has been applied in the adsorption of gaseous pollutants, *e.g.*, toluene

547 and CO$_2$, as basic N-doped biochar surface can facilitate its adsorptive behaviour towards nonpolar

548 or weakly polar gaseous substances due to electron pair donation (Jin et al., 2020; Wang et al.,

549 2019b). The increased basicity from introduced pyridinic N and pyrrolic N significantly increased

550 the adsorption capabilities of various N-doped biochars (AP-900, 496.2 mg g^{-1}; UP-900, 364.1 mg

551 g^{-1}; APP-900, 444.9 mg g^{-1}) towards toluene (Zhou et al., 2018), which was consistent with that

552 reported in CO$_2$ sequestration (AMBC, 10.15 mmol g^{-1}) by N-doped biochar beads (Nguyen and

553 Lee, 2016).

554 **4.2. Advanced oxidation processes**

555   Compared with pollutant adsorption, advanced oxidation processes (AOPs) have the potential

556 to reach complete mineralization of organics by the use of catalysts and oxidizing agents (e.g.,

557 peroxides and ozone) under appropriate reaction conditions. Since the emergence of persulfate-

558 based AOPs as a robust system to *in-situ* degrade organic contaminants in soil and groundwater, a

559 myriad of carbonaceous materials has been widely applied as metal-free peroxide activators

560 (Wang et al., 2020). Crystalline nanocarbons, including graphene and CNTs, are most frequently

561 studied owing to their superior electrochemical properties (*i.e.*, lower internal resistance and

562 energy barrier) (Duan et al., 2015e). Biochar-based materials were not considered until recent years

563 due to their structural complexity (*i.e.*, high amorphous content) and nonstoichiometric nature (*i.e.*,

564 inferior doping efficiency and weaker electrocatalysis).

565   In environmental decontamination, the common active sites on engineered biochar are electron-

566 rich structures, such as inherent functionalities, environmental persistent free radicals (EPFRs),

567 and incorporated metal centres. Nevertheless, the conventional redox-active functionalities are

568   found to be easily consumable and prone to be irreversibly oxidized after reaction (Li et al., 2020).

569   It is also generally deemed that the EFPRs and metal contents can induce uncontrollable

570   environmental implications of great human health concern when released into the ecosystem (Pan

571   et al., 2019; Ruan et al., 2019). In contrast, the N-dopants are regarded as environmentally friendly

572   and cost-effective as the concerned synthesis protocols and feedstocks are recognized to be green

573   and abundantly available, which falls into the concept of bioresource recycling scope consistent

574   with biochar production. The unveiling of graphitic biochar fabricated under high temperature (>

575   700 °C) effectively broadened the application of biochar, as unproductive amorphous carbon

576   contents can be converted to graphitic basal plane and N-dopants are readily consolidated into

577   carbon lattice under specific thermal conditions. In the meantime, the unique properties of biochar,

578   such as high oxygen contents and structural defects, can be reciprocally leveraged to promote the

579   accommodation of N atoms into carbon lattice.

580   It is well accepted that pyridinic N and graphitic N are more desired in catalytic reactions (Xie

581   et al., 2020). As aforementioned, the introduction of pyridinic N and graphitic N onto biochar

582   could disrupt the electronic properties of the original biochar framework. As depicted in **Fig. 4**,

583   pyridinic N possesses unpaired electrons that can serve as confined radicals to directly capture the

584   peroxide molecules with high electrophilic feature (Duan et al., 2016; Duan et al., 2018), while

585   graphitic N with *n*-type conduction increases the overall reactivity of localized carbon region

586   towards electron-acceptor oxyanions (Zaeni et al., 2020). Owing to the different electronegativity

587   between N and C atoms, the peroxide molecules could be adsorbed on positively charged adjacent

588   C atoms and then accept the electrons delivered from N centres. In the presence of N-dopants, this

589   integrated adsorption-activation process can lower the energy threshold of the peroxide O–O bond

590   required to be dissociated/cleaved (Duan et al., 2018).

591   Intriguingly, mild and sustainable catalysis (*i.e.*, singlet oxygenation or direct electron transfer)

592   is ubiquitous in peroxide activation using N-doped biochar, which follows a fascinating non-

593   radical mechanism distinct from those conventional radical-based oxidation processes. This

594   process is a carbon/peroxide interfacial process rather than that releases radicals into the bulk

595   solution. Accordingly, milder and sustainable mechanisms can be delivered to avoid the

596   shortcomings from non-selective radicals that might lead to the irreversible carbon surface

597   oxidative erosion or the generation of highly halogenated products, promising better recyclability

598   and sustainable operational potential of biochar. Furthermore, non-radical catalytic reaction pauses

599   when pollutant molecules are depleted, and chemical input can be reduced by preserving excessive

600   peroxide molecules for future use (Oh and Lim, 2019). In this regard, increasing attention are being

601   paid to this metal-free technology to fabricate more efficient carbocatalysts.

602   Since graphitic N-doped biochar (N-BC900, **Fig. 2b-e**) was first fabricated at ultrahigh

603   temperature (900 ℃) to activate PDS molecules for the degradation of various organics (*e.g.*,

604   orange G), the well-ordered biochar structure was found to possess high adsorption affinity

605   towards both PDS and organic molecules to provide an ideal carbon substrate with high

606   conductivity for electrochemical interactions (Zhu et al., 2018). The excellent electroactive

607   interface of N-doped biochar subsequently triggered an integral $^1O_2$ and electron transfer regime

608   (surface-confined activated metastable complex) to degrade organics *via* a non-radical pathway.

609   A similar phenomenon was elaborated in the PMS system activated by N-doped biochar derived

610   from lignocellulosic biowaste for bisphenol A degradation in **Fig. S1d** (Oh et al., 2018). Compared

611   with the symmetric PDS molecules ($^-O_3SO–OSO_3^-$), PMS (HO–OSO$_3^-$) is more susceptible to

612   electrophilic attack due to its longer peroxide O–O bond (l_{o-o}=1.453 Å) and unstable asymmetric

613   structure (Wu et al., 2020).

614   The correlation between N bonding configuration and catalytic stability was unveiled, whereby

615   graphitic N manifested higher catalytic activity and stability in contrast to pyridinic N and pyrrolic

616   N. The recovery of graphitic N from pyridinic N could be achieved by implementing high-

617   temperature annealing (*i.e.*, 800–1000 °C) at the expense of overall N level. The generation of $^1O_2$

618   in the peroxide activation was supported by several studies on other N-doped biochars (Ding et al.,

619   2020; Ma et al., 2019; Wan et al., 2020b), as graphitic N could confine PDS/PMS molecules as

620   metastable complex to prompt the self-decomposition of peroxide molecules (**Eq. 4**). Besides, the

621   formed surface-confined complex can follow another electron transfer regime to directly oxidize

622   co-adsorbed organic pollutants (Ho et al., 2019). Specifically, the electrons delivered from co-

623   adsorbed electron-rich organics could transport through highly graphitized *sp²*-hybridized carbon

624   framework to the activated oxyanion/carbon complex with the difference of their inherent redox

625   potentials as a driving force. This phenomenon is frequently reported in heteroatoms-doped

626   nanocarbons (Duan et al., 2015f; Ortiz-Medina et al., 2019), which confirmed the critical role of

627   conductive well-developed carbon π-electron network.

628   $R-N\cdots O-O_3SO^- + O-OSO_3^{2-} \rightarrow R-N +HSO_4^- + SO_4^{2-} + {}^1O_2$ (**Eq. 4**)
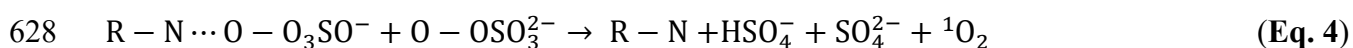
629   Although the formation of surface-confined complex on N-doped biochar is regarded as the

630   initial step in non-radical peroxide activation, most studies found the catalytic degradation in AOPs

631   should be a hybrid process consisting of both radical and non-radical pathways due to the

632   inevitable participation of other electroactive components (Xie et al., 2020; Xu et al., 2020; Zaeni

633   et al., 2020). Similarly, the participation of metals would increase the contributions of radical

634   pathways in the degradation as transition metals energetically showed higher reactivity than non-

635   metal atoms in the electrochemical process (Liu et al., 2019b; Rong et al., 2019; Zhong et al.,

636   2020), while metal-free catalysis is always recommended as a prior choice owing to its

637   environmentally benign feature. As shown in **Table 4**, the operational parameters (*e.g.*, catalyst

638   loading, peroxide dosage, and pH) significantly influenced the reaction constant rate.

639   **4.3.Energy storage and conversion**

640   Global warming, environmental deterioration, and energy shortage in the current fossil fuel

641   society have led to an ecological crisis. The storage and conversion from renewable and abundant

642   sources (*i.e.*, sun, wind, water, geothermal, and biomass) could be a rational option to relieve this

643   issue. N-doped biochar materials have shown great potential in energy storage and conversion

644   fields owing to their outstanding tunable surface chemistry and electrochemical properties.

645   Typically, N-doped biochar as a prospect electrocatalyst also extended their applications in

646   accomplishing electrochemical reduction (Yao et al., 2020), electrochemical detection (Liu et al.,

647   2020), aqueous aluminium/air battery (Wang et al., 2015b), lithium-sulphur batteries (Li et al.,

648   2019b), alkaline fuel cell (Borghei et al., 2017), and hydrogen evolution reaction (An et al., 2018;

649   Zhou et al., 2015).

650   **4.3.1. Oxygen electrocatalysts**

651   Oxygen reduction reaction (ORR) is one of the most important reactions occurring in

652   electrochemical energy storage and conversion processes, including fuel cell, water splitting, and

653   metal-air batteries. Given that the efficiency of ORR is notably restricted by the sluggish reaction

654   rate of oxygen species and high inner energy barrier, high-performance and cost-effective catalysts

655   are highly desired to meet the demands for up-scaling commercial applications. Conventional

656   oxygen electrocatalysts using noble metal (*e.g.*, Pt, Pd, and Ru) show many demerits such as low

657   abundance on earth, high cost in fabrication procedure, and reduced tolerance towards CO and

658   methanol. Given that the initial oxygen adsorption or the electron transport to the adsorbed oxygen

659   species is regarded as the rate-limiting step in ORR, N-doped biochar with a high density of active

660   sites and excellent extrinsic properties emerges as a rational alternative in the development of ORR

661   electrocatalyst.

662   As shown in **Fig. S4** , Liu et al. (2015a) fabricated a N self-doped electrocatalyst derived from

663   water hyacinth for ORR. The onset potential was calculated to be +0.98 V *vs.* reversible hydrogen

664   electrode (RHE), which was even more positive than that of commercial Pt/C (+0.95 V). The

665   superior electrochemical properties were attributed to the abundant pyridinic N and graphitic N,

666   as the lone-pair electrons from N-dopants can help to activate carbon π electrons for better

667   adsorption of oxygen molecules and lead to higher conductivity. Liang et al. (2018) also employed

668   water hyacinth biowaste to produce N-doped biochar in the $2e^-$ ORR for the generation of

669   hydrogen peroxide (H_2O_2). The yield of H_2O_2 and current efficiency could be elevated to 1.7 mmol

670   L^{-1} and 81.2%, respectively, compared with the pristine biochar without N-dopants (1.1 mmol L^{-1}

671   ^{1} and 28.3%). It could be concluded that the introduced N-dopants on biochar can act as

672   electroactive sites to promise faster electron migration. As shown in **Table 5**, several other N-

673   doped biochars were reported to be remarkably effective for ORR in both acidic and alkaline

674   environment. Most of them showed a comparable onset potential and half-wave potential to those

675   of costly commercial 20 *wt*.% Pt/C. Furthermore, the N-doped biochar appeared to be more

676   tolerable towards methanol with a higher longer-term stability compared with noble metal

677   electrodes (Borghei et al., 2017; Chen et al., 2014; Liu et al., 2014).

678   Interestingly, the active sites on N-doped biochar electrocatalysts all indexed to pyridinic N and

679   graphitic N. This phenomenon coincides with the conclusion drawn in previous parts, as pyridinic

680   N and graphitic N are regarded to be electroactive sites with highest electrochemical reactivity in

681   redox reactions. SSA is also a key parameter to determine the reactivity of electrocatalysts, which

682   is conducive to the fast mass transfer and electron migration (Pan et al., 2014). The decomposition

683   of various N precursors can result in higher SSA, uniform N-doping, and a well-developed porous

684   structure, which intimately match with the desired characteristics of ORR electrocatalysts.

685   Simultaneous incorporation of transition metal contents is another appealing strategy to obtain

686   high-performance ORR catalysts. The participation of metal contents was found to catalyse the

687   formation of N-dopants apart from their direct contribution as Lewis basic sites in ORR (Pi et al.,

688   2020; Zhang et al., 2017).

689   Oxygen evolution reaction (OER) is another electrocatalytic process for energy storage and

690   conversion featured as a four-electron process associated with applications in water splitting and

691   rechargeable metal-air batteries. Due to its sluggish nature from low reaction kinetics, the oxygen

692   electrocatalyst with excellent electrochemical capacities is essential to accelerate the OER rate and

693   reduce overpotential. Similar to ORR, N-doped biochar based electrocatalyst could be a suitable

694   candidate to replace the conventional noble metal catalyst (*e.g.*, IrO_2 and RuO_2) in OER owing to

695   its high catalytic activity and excellent stability (Liu et al., 2019c). As shown in **Fig. S5**, Wang et

696   al. (2017) fabricated a biochar-based material derived from *Chlorella,* and the synthesized

697   electrocatalyst showed high performance in both ORR and OER. Apart from the favourable ORR

698   half-wave potential at 0.84 V, which transcended that of commercial 20 *wt.*% Pt/C (0.83 V), its

699   OER overpotential at 10 mA cm^{-2} was 23 mV, also lower than the reference electrode IrO_2/C in

700   1.0 M KOH solution. Such a bifunctional feature was attributed to the simultaneous enrichment of

701   pyridinic N and graphitic N as predominant active sites in ORR and OER, respectively.

702   **4.3.2. Microbial fuel cell**

703   Different from ORR and OER that rely on external power to initiate the reaction, microbial fuel

704   cells (MFCs) is another technology that converts the organic or inorganic contaminants into

705   electrical energy through the spontaneous metabolism of microbes (Wang et al., 2018b). The

706   selection of electrode material is crucial in MFCs as it greatly influences the biofilm formation,

707   inner energy barrier/resistance, and enrichment of pollutant molecules, *etc*. Considering that MFCs

708   are mainly designed for practical wastewater treatment, the ideal electrode material applied in

709   MFCs should possess superior electrochemical properties with relatively low prices, and

710   meanwhile, is required to be biocompatible, durable, and environmentally friendly under microbial

711   stress. In this regard, sustainable N-doped biochar can be an excellent precursor for manufacturing

712   the cathodic electrode for MFCs.

713   Biochar derived from milling residue showed a peak power output at 532 ± 18 mW m^{-2} in MFC

714   comparable to those assigned to AC and graphite granule at 674 ± 10 and 566 ± 5 mW m^{-2},

715   respectively (Huggins et al., 2014). Furthermore, the material cost for biochar preparation (0.051–

716   0.381 US\$ g^{-1}) was nearly 90% lower than its carbon counterparts (0.8–2.5 US\$ g^{-1} for AC and

717   0.5–0.8 US\$ g^{-1} for graphite granule). As mentioned above, the participation of N-doping could

718   significantly enhance the electrochemical properties with a relatively low increase in reagent cost.

719   As shown in **Fig. S6**, Zhong et al. (2019b) fabricated N-doped biochar derived from watermelon

720   rind as a cathode material. The as-prepared N-doped biochar possessed a current density and

721   charge transfer resistance of 0.19 mA cm^{-2} and 20.6 Ω comparable to those of commercial Pt/C

722   catalyst (0.20 mA cm^{-2} and 37.6 Ω). Compared with graphitic biochar (146.7 mW m^{-2}, 0.0004

723   US\$ g^{-1}), the power density of N-doped biochar could reach 262.0 mW m^{-2} while the price only

724   increased to 0.015 US\$ g^{-1}, which was economically superior to commercial Pt/C (512 mW m^{-2},

725   33US\$ g^{-1}) (Huggins et al., 2015).

726   Another N-doped biochar derived from cellulose paper with an ultra-high surface area of 1170.6

727   m^2 g^{-1} was applied in MFCs (Yue et al., 2015). The maximum power density in this N-doped

728   biochar/MFC system reached 1041 ± 90 mW m^{-2}, which was much higher than that of Pt/C-based

729   MFC (584 ± 10 mW m^{-2}). Noteworthily, Liu et al. (2015b) found the co-doping of phosphate using

730   ammonium phosphate as N/P source could achieve an ultrahigh maximum power density at 2293

731   ± 50 mW m^{-2} in the N, P-doped biochar MFC system, which might suggest the great potential for

732   co-doping technology in MFCs. As shown in **Table 6**, the key N-dopants pointed to pyridinic N

733   and graphitic N, further confirming their critical role in electrochemical reactions.

734   **4.3.3. Energy storage vessels**

735   In principle, there is no fundamental difference among biochar, activated carbon, and carbon

736   black, except that biochar surface is usually rich in functional groups. Since the establishment of

737   geobattery theory, *i.e.*, quinone/hydroquinone pairs can undergo reversible functional interspecies

738   conversion on carbonized matrix (Klüpfel et al., 2014; Sun et al., 2017), the potential of utilizing

739   biochar to fabricate energy storage vessels is unveiled.

740   Supercapacitor offers a fascinating approach to store clean/renewable energy and stands out due

741   to its high power density, efficient reversibility, and good recyclability (Miller and Simon, 2008).

742   With the highly scalable surface chemistry by selecting specific biomass precursors, thermal

743   conditions, and modification methods, biochar has been experimented to produce high energy

744   density supercapacitor. Biswal et al. (2013) produced biochar by single-step pyrolysis of dead plant

745   leaves with a high surface area of ~1230 m^2 g^{-1}. The synthesized biochar showed a respectable

746   specific capacitance of 400 F g^{-1} and an energy density of 55 W h kg^{-1} at a current density of 0.5

747   A g^{-1} in acidic electrolyte. The enhanced energy storage efficiency was ascribed to the introduction

748   of N-dopants into biochar. Li et al. (2012) synthesized a supercapacitor electrode material using

749   chicken eggshell membranes, and excellent specific capacitances of 297 and 284 F g^{-1} could be

750   achieved in both basic and acidic electrolytes, respectively. This favourable electrochemical

751   capacity was because of the redox reactions between N-dopants and oxygen functionalities. Liu et

752 al. (2016) fabricated a porous N-rich carbon from sugar cane bagasse and urea with 323 and 213

753 F g^{-1} at the discharge/charge current densities of 1 and 30 A g^{-1}, respectively. Abundant porosities

754 were found to conduce ion buffering and accommodation while high N content could notably

755 increase the pseudocapacitance.

756 In the view of chemistry, the pyridinic N or pyrrolic N adjacent to a quinone oxygen atom is

757 regarded as primary N-dopants contributing to the supercapacitor capacitance (Hulicova-

758 Jurcakova et al., 2009), while graphitic N can accelerate the electron migration and introduce

759 pseudocapacitance *via* the interaction with protons in an acidic electrolyte (Lee et al., 2013).

760 Similar to foregoing applications, the co-doping technology also demonstrated a combined effect

761 from the co-existence of N and S to improve the specific capacitance and cycling performance of

762 banana-derived biochar supercapacitor (Wang et al., 2014).

763 **4.3.4. Biofuel production**

764 The conversion of biomass or CO_2 to value-added chemical products is one of the emerging

765 applications of biochar (Cao et al., 2019; Xiong et al., 2017), which could provide an alternative

766 method to alleviate the energy shortage in the current fossil fuel society. Value-added chemical

767 production involves a series of reactions initiating with the saccharification of glucans to glucose.

768 Subsequently, the produced glucose can be isomerised to fructose, which can be further upgraded

769 to useful platform chemicals, such as hydroxymethylfurfural (HMF) (Yu et al., 2016).

770 Isomerisation of glucose to fructose relies on Lewis acid (electron pair acceptor) *via* catalytic

771 routes through a hydride shift from C2 to C1 or a hydrogen transfer from O2 to O1 of glucose,

772 respectively (Binder et al., 2010; Yu et al., 2019b). As shown in **Fig. 5**, Chen et al. (2018b)

773 fabricated a useful biochar catalyst derived from spent coffee grounds with melamine for the

774 isomerization of glucose to fructose. Fast glucose conversion (12%) and high selectivity to fructose

775 (84%) could be reached at a moderate temperature of 120 °C within 20 min. The coffee-derived

776 biochar was superior in selecticity compared with conventional catalysts, including aqueous

777 hydroxides and amines (50−80% to fructose) with comparable catalytic activity (~20 mol%

778 conversion within 20 min). Pyridinic N was regarded as the main catalytic site owing to its

779 localized lone pair and nucleophilic nature.

780 The methanation of CO_2 to produce CH_4 is receiving tremendous attention because it could reach

781 the sequestration of CO_2 and the generation of biofuel simultaneously (Dreyer et al., 2017). The

782 most commonly used active catalysts for methanation are noble metals (*e.g.*, Ru, Rh, Pt, and Pd).

783 Although these metals are catalytically active, they must be deposited onto inert supports to avoid

784 sintering and aggregation. The evolvement of N-doped biochar can provide an economical carbon

785 substrate. The abundant basic N-dopants can afford electron pair donation to promise high

786 catalysis and suppress the deactivation of metal centres caused by coke deposition (Roldán et al.,

787 2017). Wang et al. (2019b) produced N-doped biochar derived from *Pinus Sylvestris* with urea as

788 Ru support. The generated catalyst could achieve a high CO_2 conversion rate of 93.8% and a CH_4

789 selectivity of 99.7%. The basic N-dopants (mainly pyridinic N and pyrrolic N) could serve as an

790 electron donor to promote the Ru incorporation and anchoring sites for CO_2 adsorption to enhance

791 the conversion.

792 **4.4. Limitations of N-doped biochar in environmental and energy applications**

793 N-doping technology gives a great boost to biochar for its high performances on contaminant

794 adsorption and catalytic remediation; however, the ideal regeneration protocols are not well

795 coordinated by which nitorgen dopants can be readily refreshed without drastic chemical/energy

796 input. The introduced N-dopants will establish an electron-paired bonding towards adsorbed

797 organics with irreversible features (Oh and Lim, 2019). Zhang (2019) claimed that the activity can

798   be partially recovered *via* simple annealing at 800 ℃, while an annealing temperature higher than

799   800 ℃ to evaporate/carbonize adsorbates and oxidized contents would cause the attenuation of N

800   active sites. Wan et al. (2020b) employed a low-temperature treatment (250 ℃) to restore the

801   catalytic capability of N-doped biochar; however, this strategy was limited to remove organics

802   with low evaporation points. More emerging methods (*e.g.*, sonication, microwave, hydorthemal

803   treatment) with lower energy input can be explored to restore the active region of N-doped biochar

804   in future work.

805   Furthermore, the correlation between the density of N-dopants and electrocatalytic performance

806   remains unclear, as many researchers claimed that no relation was found between total N level and

807   electrochemical activity (Nagaiah et al., 2010; Oh et al., 2011). Based on the current state of

808   knowledge, only organics with simple molecular structure, lower ionized potential (< 9.0 eV), and

809   abundant electron-rich functionalities (*e.g.*, amino and hydroxy groups) could be decomposed *via*

810   non-radical pathway (Duan et al., 2019; Hu et al., 2017). To meet specific practical demands,

811   diversity of pollutant selection should be taken into consideration in the future study.

812   At the present stage, the research on heteroatoms co-doped biochar is still not sufficient to reach

813   a definite conclusion. More relevant studies are encouraged since co-doping technology has been

814   proven effective on other carbon platforms (Duan et al., 2015d; Tian et al., 2016). Ding et al. (2020)

815   manufactured several N-doped, S-doped, and N, S-doped biochars to verify the synergies between

816   different non-carbon heteroatoms, and found only N-doping exerted positive effects on the

817   catalytic capacities of resultant biochar. The co-doping mechanism on biochar-based

818   electrocatalyst fabrication is also inadequately explored, although density functional theory (DFT)

819   calculations verified that the co-doping of another non-carbon atom could further alter the

820   electronic nature of carbon matrix to increase its catalytic activity (Zhou et al., 2015).

821   Besides, the combination between N-doped biochar and MFCs needs further elaboration from

822   mechanistic aspects. Notably, the influences of basic N-dopants on the material compatibility,

823   microbe acclimation, electron transfer mechanism, synergies between electrode adsorption and

824   biofilm, and long-term stability are yet to be revealed and should be addressed in the future study.

825   Also, future work should focus on the advantage of the easily tunable features of heteroatoms-

826   doped biochar to fabricate high-performance supercapacitors with well-developed porosities,

827   electrical conductivity, and excellent durability towards electrolyte.

828

829   **5. Conclusion**

830   In this review, recent advances in the fabrications and applications of N-doped biochar are

831   summarised and discussed. Generally, the superior electrochemical properties, versatile porous

832   structure, and higher surface area of N-doped biochar can be achieved by selecting specific doping

833   techniques and controlling the operational conditions during production. The green and sustainable

834   nature of the N-doping technique are in alignment with the biochar production with low

835   environmental concern. The abundant electroactive N-dopants make N-doped biochar a

836   prospective alternative in various environmental and energy applications such as adsorption,

837   catalytic decontamination, energy storage, and biofuel production to replace the conventional

838   metal-based catalysts. In particular, a comprehensive understanding of the doping mechanism and

839   the characteristics of each N-dopants elaborated in this work propel the field of biochar to further

840   apply this appealing material for more novel sustainable carbocatalysis in the future.

841

842   **6. Perspectives**

843   For directions of future study on N-doped biochar, several aspects can be further explored: (a)

844   The importance of the self-doping technique should be highlighted in future N-doped biochar

845   production. Combined with plant biotechnology, eutrophic elements recycle and biomass disposal

846   can be simultaneously achieved by intaking heteroatoms precursor into biomass prior to

847   carbonization as a sustainable method; (b) Rational manipulation of types and densities of N-

848   dopants during production and applications should be explored and optimized, while the present

849   studies lack the emphasis on the fate of N-dopants and their environmental implications; (c) The

850   co-existing impurities that are unlikely to be removed entirely from biomass, especially

851   endogenous metal contents, will lead to nonnegligible effects on the physicochemical properties

852   (*i.e.*, carbon structure, N-dopants, defective level, and graphitic degree) of resultant N-doped

853   biochar. Relevant research could provide a systematic investigation on the influence of these

854   impurities by selecting specific biomass or adding additives, and compare with other simplified

855   carbonaceous material with similar carbon structure, *e.g.*, AC; (d) The full illustration of the doping

856   mechanism remains a challenge. *In-situ* advanced characterization and computational modeling

857   could help to construct a fundamental scheme. Considering the paramagnetic properties of N-

858   dopants with unpaired electrons, combining the electron paramagnetic spectroscopic (EPR)

859   characteristic signals and DFT calculations might be a promising approach to reveal the formation

860   and compositions of N-dopants; (e) Metal-free carbonaceous materials usually exhibit lower

861   stability when exposed to harsh conditions. The stability and efficiency of N-doped biochar should

862   be optimized combined with the exploration of co-doping technology. The regeneration of spent

863   N-doped biochar also requires more concentration; (f) Given the sustainable and economic features

864   of N-doped biochar, future work could focus more on the non-radical degradation, biorefinery, and

865   fabrication of energy storage devices to expand its role in green and sustainable chemistry. The

866   current progress of N-doped biochar in environmental fields triggers inspiring accomplishment.

867 With continuous contributions to promoting this material, up-scaling practical applications of N-

868 doped biochar can give impetus to the value-added utilization of renewable bioresource.

869

873

874 **References**

875 [1] J.S. Cha, S.H. Park, S.-C. Jung, C. Ryu, J.-K. Jeon, M.-C. Shin, Y.-K. Park, Production and

876 utilization of biochar: A review, Journal of Industrial and Engineering Chemistry, 40 (2016) 1-15.

877 [2] X. Xiong, I.K.M. Yu, L. Cao, D.C.W. Tsang, S. Zhang, Y.S. Ok, A review of biochar-based

878 catalysts for chemical synthesis, biofuel production, and pollution control, Bioresource technology,

879 246 (2017) 254-270.

880 [3] I. Anastopoulos, I. Pashalidis, A. Hosseini-Bandegharaei, D.A. Giannakoudakis, A. Robalds,

881 M. Usman, L.B. Escudero, Y. Zhou, J.C. Colmenares, A. Núñez-Delgado, É.C. Lima, Agricultural

882 biomass/waste as adsorbents for toxic metal decontamination of aqueous solutions, Journal of

883 Molecular Liquids, 295 (2019) 111684.

884 [4] A. Demirbaş, Mechanisms of liquefaction and pyrolysis reactions of biomass, Energy

885 Conversion & Management, 41 (2000) 633-646.

886 [5] J. Li, J. Dai, G. Liu, H. Zhang, Z. Gao, J. Fu, Y. He, Y. Huang, Biochar from microwave

887 pyrolysis of biomass: A review, Biomass and Bioenergy, 94 (2016) 228-244.

888 [6] D.-W. Cho, K. Yoon, Y. Ahn, Y. Sun, D.C.W. Tsang, D. Hou, Y.S. Ok, H. Song, Fabrication

889 and environmental applications of multifunctional mixed metal-biochar composites (MMBC)

890   from red mud and lignin wastes, Journal of hazardous materials, 374 (2019) 412-419.

891   [7] Q. Xu, Z. Chen, Z. Wu, F. Xu, D. Yang, Q. He, G. Li, Y. Chen, Novel lanthanum doped

892   biochars derived from lignocellulosic wastes for efficient phosphate removal and regeneration,

893   Bioresource technology, 289 (2019a) 121600.

894   [8] J. Lee, X. Yang, S.-H. Cho, J.-K. Kim, S.S. Lee, D.C.W. Tsang, Y.S. Ok, E.E. Kwon,

895   Pyrolysis process of agricultural waste using CO2 for waste management, energy recovery, and

896   biochar fabrication, Applied Energy, 185 (2017a) 214-222.

897   [9] M. Tripathi, J.N. Sahu, P. Ganesan, Effect of process parameters on production of biochar

898   from biomass waste through pyrolysis: A review, Renewable & Sustainable Energy Reviews, 55

899   (2016) 467-481.

900   [10] A.D. Igalavithana, S. Wan Choi, P.D. Dissanayake, J. Shang, C.-H. Wang, X. Yang, S. Kim,

901   D.C.W. Tsang, K.B. Lee, Y.S. Ok, Gasification biochar from biowaste (food waste and wood

902   waste) for effective CO2 adsorption, Journal of hazardous materials, (2019) 121147.

903   [11] X. Yang, A. Tsibart, H. Nam, J. Hur, A. El-Naggar, F.M.G. Tack, C.-H. Wang, Y.H. Lee,

904   D.C.W. Tsang, Y.S. Ok, Effect of gasification biochar application on soil quality: Trace metal

905   behavior, microbial community, and soil dissolved organic matter, Journal of hazardous materials,

906   365 (2019a) 684-694.

907   [12] S. You, Y.S. Ok, S.S. Chen, D.C.W. Tsang, E.E. Kwon, J. Lee, C.-H. Wang, A critical

908   review on sustainable biochar system through gasification: Energy and environmental applications,

909   Bioresource technology, 246 (2017) 242-253.

910   [13] P. Gao, D. Yao, Y. Qian, S. Zhong, L. Zhang, G. Xue, H. Jia, Factors controlling the

911   formation of persistent free radicals in hydrochar during hydrothermal conversion of rice straw,

912   Environmental Chemistry Letters, 16 (2018) 1463-1468.

913   [14] J. Wang, S. Wang, Preparation, modification and environmental application of biochar: A

914   review, Journal of Cleaner Production, 227 (2019) 1002-1022.

915   [15] D.-W. Cho, G. Kwon, K. Yoon, Y.F. Tsang, Y.S. Ok, E.E. Kwon, H. Song, Simultaneous

916   production of syngas and magnetic biochar via pyrolysis of paper mill sludge using CO2 as

917   reaction medium, Energy Conversion and Management, 145 (2017) 1-9.

918   [16] M.-T. Yang, Y. Du, W.-C. Tong, A.C.K. Yip, K.-Y.A. Lin, Cobalt-impregnated biochar

919   produced from CO2-mediated pyrolysis of Co/lignin as an enhanced catalyst for activating

920   peroxymonosulfate to degrade acetaminophen, Chemosphere, 226 (2019b) 924-933.

921   [17] K.N. Palansooriya, Y.S. Ok, Y.M. Awad, S.S. Lee, J.-K. Sung, A. Koutsospyros, D.H.

922   Moon, Impacts of biochar application on upland agriculture: A review, Journal of environmental

923   management, 234 (2019) 52-64.

924   [18] M. Fowles, Black carbon sequestration as an alternative to bioenergy, Biomass and

925   Bioenergy, 31 (2007) 426-432.

926   [19] H. Bamdad, K. Hawboldt, S. Macquarrie, A review on common adsorbents for acid gases

927   removal: Focus on biochar, Renewable & Sustainable Energy Reviews, 81 (2017)

928   S1364032117309152.

929   [20] M. Kumar, X. Xiong, Y. Sun, I.K.M. Yu, D.C.W. Tsang, D. Hou, J. Gupta, T. Bhaskar, A.

930   Pandey, Critical Review on Biochar-Supported Catalysts for Pollutant Degradation and

931   Sustainable Biorefinery, Advanced Sustainable Systems, (2020) 1900149.

932   [21] J. Lee, K.-H. Kim, E.E. Kwon, Biochar as a Catalyst, Renewable & Sustainable Energy

933   Reviews, 77 (2017b) 70-79.

934   [22] Z. Wan, D.-W. Cho, D.C.W. Tsang, M. Li, T. Sun, F. Verpoort, Concurrent adsorption and

935   micro-electrolysis of Cr(VI) by nanoscale zerovalent iron/biochar/Ca-alginate composite,

936   Environmental Pollution, 247 (2019a) 410-420.

937   [23] Z. Wan, Y. Sun, D.C.W. Tsang, I.K.M. Yu, J. Fan, J.H. Clark, Y. Zhou, X. Cao, B. Gao,

938   Y.S. Ok, A sustainable biochar catalyst synergized with copper heteroatoms and CO2 for singlet

939   oxygenation and electron transfer routes, Green Chemistry, 21 (2019b) 4800-4814.

940   [24] X. Li, L. Liu, X. Wang, Y.S. Ok, J.A.W. Elliott, S.X. Chang, H.-J. Chung, Flexible and

941   Self-Healing Aqueous Supercapacitors for Low Temperature Applications: Polyampholyte Gel

942   Electrolytes with Biochar Electrodes, Scientific reports, 7 (2017) 1685.

943   [25] M. Ahmad, A.U. Rajapaksha, J.E. Lim, M. Zhang, N. Bolan, D. Mohan, M. Vithanage, S.S.

944   Lee, Y.S. Ok, Biochar as a sorbent for contaminant management in soil and water: A review,

945   Chemosphere, 99 (2014) 19-33.

946   [26] F. Beckers, Y.M. Awad, J. Beiyuan, J. Abrigata, S. Mothes, D.C.W. Tsang, Y.S. Ok, J.

947   Rinklebe, Impact of biochar on mobilization, methylation, and ethylation of mercury under

948   dynamic redox conditions in a contaminated floodplain soil, Environment International, 127 (2019)

949   276-290.

950   [27] A. El-Naggar, S.S. Lee, J. Rinklebe, M. Farooq, H. Song, A.K. Sarmah, A.R. Zimmerman,

951   M. Ahmad, S.M. Shaheen, Y.S. Ok, Biochar application to low fertility soils: A review of current

952   status, and future prospects, Geoderma, 337 (2019) 536-554.

953   [28] X. Chen, W.-D. Oh, T.-T. Lim, Graphene- and CNTs-based carbocatalysts in persulfates

954   activation: Material design and catalytic mechanisms, Chemical Engineering Journal, 354 (2018a)

955   941-976.

956   [29] H. Sun, S. Liu, G. Zhou, H.M. Ang, M.O. Tadé, S. Wang, Reduced Graphene Oxide for

957   Catalytic Oxidation of Aqueous Organic Pollutants, ACS applied materials & interfaces, 4 (2012)

958   5466-5471.

959   [30] H. Lee, H.I. Kim, S. Weon, W. Choi, Y.S. Hwang, J. Seo, C. Lee, J.H. Kim, Activation of

960   Persulfates by Graphitized Nanodiamonds for Removal of Organic Compounds, Environmental

961   science & technology, 50 (2016) 10134.

962   [31] X. Duan, H. Sun, S. Wang, Metal-Free Carbocatalysis in Advanced Oxidation Reactions,

963   Accounts of Chemical Research, 51 (2018) 678.

964   [32] A.L. Cazetta, A.M.M. Vargas, E.M. Nogami, M.H. Kunita, M.R. Guilherme, A.C. Martins,

965   T.L. Silva, J.C.G. Moraes, V.C. Almeida, NaOH-activated carbon of high surface area produced

966   from coconut shell: Kinetics and equilibrium studies from the methylene blue adsorption,

967   Chemical Engineering Journal, 174 (2011) 117-125.

968   [33] A.U. Rajapaksha, S.S. Chen, D.C.W. Tsang, M. Zhang, M. Vithanage, S. Mandal, B. Gao,

969   N.S. Bolan, Y.S. Ok, Engineered/designer biochar for contaminant removal/immobilization from

970   soil and water: Potential and implication of biochar modification, Chemosphere, 148 (2016) 276-

971   291.

972   [34] F. Yang, S. Zhang, Y. Sun, K. Cheng, J. Li, D.C.W. Tsang, Fabrication and characterization

973   of hydrophilic corn stalk biochar-supported nanoscale zero-valent iron composites for efficient

974   metal removal, Bioresource technology, 265 (2018) 490-497.

975   [35] F. Yang, S. Zhang, Y. Sun, D.C.W. Tsang, K. Cheng, Y.S. Ok, Assembling biochar with

976   various layered double hydroxides for enhancement of phosphorus recovery, Journal of hazardous

977   materials, 365 (2019c) 665-673.

978   [36] Y. Yi, Z. Huang, B. Lu, J. Xian, E.P. Tsang, W. Cheng, J. Fang, Z. Fang, Magnetic biochar

979   for environmental remediation: A review, Bioresource technology, 298 (2020) 122468.

980   [37] H. Wang, B. Gao, S. Wang, J. Fang, Y. Xue, K. Yang, Removal of Pb(II), Cu(II), and Cd(II)

981   from aqueous solutions by biochar derived from KMnO4 treated hickory wood, Bioresource

982   technology, 197 (2015a) 356-362.

983   [38] M.-T. Yang, W.-C. Tong, J. Lee, E. Kwon, K.-Y.A. Lin, CO2 as a reaction medium for

984   pyrolysis of lignin leading to magnetic cobalt-embedded biochar as an enhanced catalyst for Oxone

985   activation, Journal of colloid and interface science, 545 (2019d) 16-24.

986   [39] W.-D. Oh, T.-T. Lim, Design and application of heterogeneous catalysts as peroxydisulfate

987   activator for organics removal: An overview, Chemical Engineering Journal, 358 (2019) 110-133.

988   [40] J. Ortiz-Medina, Z. Wang, R. Cruz-Silva, A. Morelos-Gomez, F. Wang, X. Yao, M.

989   Terrones, M. Endo, Defect Engineering and Surface Functionalization of Nanocarbons for Metal-

990   Free Catalysis, Advanced materials, 31 (2019) 1805717.

991   [41] B. Frank, J. Zhang, R. Blume, R. Schlögl, D.S. Su, Heteroatoms Increase the Selectivity in

992   Oxidative Dehydrogenation Reactions on Nanocarbons, Angewandte Chemie International

993   Edition, 48 (2009) 6913-6917.

994   [42] Q. Yang, Z. Xiao, D. Kong, T. Zhang, X. Duan, S. Zhou, Y. Niu, Y. Shen, H. Sun, S. Wang,

995   L. Zhi, New insight to the role of edges and heteroatoms in nanocarbons for oxygen reduction

996   reaction, Nano Energy, 66 (2019e) 104096.

997   [43] S. Zhu, X. Huang, F. Ma, L. Wang, X. Duan, S. Wang, Catalytic Removal of Aqueous

998   Contaminants on N-Doped Graphitic Biochars: Inherent Roles of Adsorption and Nonradical

999   Mechanisms, Environmental science & technology, 52 (2018) 8649-8658.

1000   [44] D. Ding, S. Yang, X. Qian, L. Chen, T. Cai, Nitrogen-doping positively whilst sulfur-

1001   doping negatively affect the catalytic activity of biochar for the degradation of organic contaminant,

1002   Applied Catalysis B: Environmental, 263 (2020) 118348.

1003   [45] S.-H. Ho, Y.-d. Chen, R. Li, C. Zhang, Y. Ge, G. Cao, M. Ma, X. Duan, S. Wang, N.-q.

1004   Ren, N-doped graphitic biochars from C-phycocyanin extracted Spirulina residue for catalytic

persulfate activation toward nonradical disinfection and organic oxidation, Water research, 159 (2019) 77-86.

[46] D. Li, Y. Jia, G. Chang, J. Chen, H. Liu, J. Wang, Y. Hu, Y. Xia, D. Yang, X. Yao, A Defect-Driven Metal-free Electrocatalyst for Oxygen Reduction in Acidic Electrolyte, Chem, 4 (2018) 2345-2356.

[47] X. Liu, L. Dai, Carbon-based metal-free catalysts, Nature Reviews Materials, 1 (2016) 16064.

[48] T.S. Miller, A.B. Jorge, T.M. Suter, A. Sella, F. Corà, P.F. McMillan, Carbon nitrides: synthesis and characterization of a new class of functional materials, Physical Chemistry Chemical Physics, 19 (2017) 15613-15638.

[49] M.M. Mian, G. Liu, B. Yousaf, B. Fu, R. Ahmed, Q. Abbas, M.A.M. Munir, L. Ruijia, One-step synthesis of N-doped metal/biochar composite using NH3-ambiance pyrolysis for efficient degradation and mineralization of Methylene Blue, Journal of Environmental Sciences, 78 (2019) 29-41.

[50] M.M. Mian, G. Liu, B. Yousaf, B. Fu, H. Ullah, M.U. Ali, Q. Abbas, M.A. Mujtaba Munir, L. Ruijia, Simultaneous functionalization and magnetization of biochar via NH3 ambiance pyrolysis for efficient removal of Cr (VI), Chemosphere, 208 (2018) 712-721.

[51] X. Duan, H. Sun, Y. Wang, K. Jian, S. Wang, N-Doping-Induced Nonradical Reaction on Single-Walled Carbon Nanotubes for Catalytic Phenol Oxidation, Acs Catalysis, 5 (2015a) 553-559.

[52] K. Gao, B. Wang, L. Tao, B.V. Cunning, Z. Zhang, S. Wang, R.S. Ruoff, L. Qu, Efficient Metal-Free Electrocatalysts from N-Doped Carbon Nanomaterials: Mono-Doping and Co-Doping, Advanced materials, 31 (2019) 1805121.

1028   [53] X. Duan, Z. Ao, H. Sun, L. Zhou, G. Wang, S. Wang, Insights into N-doping in single-

1029 walled carbon nanotubes for enhanced activation of superoxides: a mechanistic study, Chemical

1030 Communications, 51 (2015b) 15249-15252.

1031   [54] H. Sun, C.K. Kwan, A. Suvorova, H.M. Ang, M.O. Tadé, S. Wang, Catalytic oxidation of

1032 organic pollutants on pristine and surface nitrogen-modified carbon nanotubes with sulfate radicals,

1033 Applied Catalysis B Environmental, 154-155 (2014) 134-141.

1034   [55] Z. Wan, Y. Sun, D.C.W. Tsang, D. Hou, X. Cao, S. Zhang, B. Gao, Y.S. Ok, Sustainable

1035 remediation with electroactive biochar system: Mechanisms and perspectives, Green Chemistry,

1036 (2020a)

1037   [56] D. Wu, W. Song, L. Chen, X. Duan, Q. Xia, X. Fan, Y. Li, F. Zhang, W. Peng, S. Wang,

1038 High-performance porous graphene from synergetic nitrogen doping and physical activation for

1039 advanced nonradical oxidation, Journal of hazardous materials, 381 (2020) 121010.

1040   [57] J. Liang, D. Tang, L. Huang, Y. Chen, W. Ren, J. Sun, High oxygen reduction reaction

1041 performance nitrogen-doped biochar cathode: A strategy for comprehensive utilizing nitrogen and

1042 carbon in water hyacinth, Bioresource technology, 267 (2018) 524-531.

1043   [58] M. Shao, Q. Chang, J.-P. Dodelet, R. Chenitz, Recent Advances in Electrocatalysts for

1044 Oxygen Reduction Reaction, Chemical Reviews, 116 (2016) 3594-3657.

1045   [59] L.-L. Ling, W.-J. Liu, S. Zhang, H. Jiang, Magnesium Oxide Embedded Nitrogen Self-

1046 Doped Biochar Composites: Fast and High-Efficiency Adsorption of Heavy Metals in an Aqueous

1047 Solution, Environmental science & technology, 51 (2017) 10081-10089.

1048   [60] X. Rong, M. Xie, L. Kong, V. Natarajan, L. Ma, J. Zhan, The magnetic biochar derived

1049 from banana peels as a persulfate activator for organic contaminants degradation, Chemical

1050 Engineering Journal, 372 (2019) 294-303.

1051   [61] W. Ma, N. Wang, Y. Du, P. Xu, B. Sun, L. Zhang, K.-Y.A. Lin, Human-Hair-Derived N,

1052 S-Doped Porous Carbon: An Enrichment and Degradation System for Wastewater Remediation in

1053 the Presence of Peroxymonosulfate, ACS Sustainable Chemistry & Engineering, 7 (2019) 2718-

1054 2727.

1055   [62] Y. Xie, W. Hu, X. Wang, W. Tong, P. Li, H. Zhou, Y. Wang, Y. Zhang, Molten salt induced

1056 nitrogen-doped biochar nanosheets as highly efficient peroxymonosulfate catalyst for organic

1057 pollutant degradation, Environmental Pollution, 260 (2020) 114053.

1058   [63] J. Liu, S. Jiang, D. Chen, L. Liu, J. Wu, Y. Shu, Activation of persulfate with biochar for

1059 degradation of bisphenol A in soil, Chemical Engineering Journal, (2019a) 122637.

1060   [64] J. Yu, L. Tang, Y. Pang, G. Zeng, J. Wang, Y. Deng, Y. Liu, H. Feng, S. Chen, X. Ren,

1061 Magnetic nitrogen-doped sludge-derived biochar catalysts for persulfate activation: Internal

1062 electron transfer mechanism, Chemical Engineering Journal, 364 (2019a) 146-159.

1063   [65] K. Luo, Q. Yang, Y. Pang, D. Wang, X. Li, M. Lei, Q. Huang, Unveiling the mechanism

1064 of biochar-activated hydrogen peroxide on the degradation of ciprofloxacin, Chemical Engineering

1065 Journal, 374 (2019) 520-530.

1066   [66] W.-D. Oh, G. Lisak, R.D. Webster, Y.-N. Liang, A. Veksha, A. Giannis, J.G.S. Moo, J.-W.

1067 Lim, T.-T. Lim, Insights into the thermolytic transformation of lignocellulosic biomass waste to

1068 redox-active carbocatalyst: Durability of surface active sites, Applied Catalysis B: Environmental,

1069 233 (2018) 120-129.

1070   [67] Z. Lin, G. Waller, L. Yan, M. Liu, C.i. Wong, Facile Synthesis of Nitrogen-Doped

1071 Graphene via Pyrolysis of Graphene Oxide and Urea, and its Electrocatalytic Activity toward the

1072 Oxygen-Reduction Reaction, Advanced Energy Materials, 2 (2012) 884-888.

1073   [68] H. Wang, W. Guo, B. Liu, Q. Wu, H. Luo, Q. Zhao, Q. Si, F. Sseguya, N. Ren, Edge-

1074 nitrogenated biochar for efficient peroxydisulfate activation: An electron transfer mechanism,

1075 Water research, 160 (2019a) 405-414.

1076 [69] J. Hou, T. Jiang, R. Wei, F. Idrees, D. Bahnemann, Ultrathin-Layer Structure of BiOI

1077 Microspheres Decorated on N-Doped Biochar With Efficient Photocatalytic Activity, Frontiers in

1078 Chemistry, 7 (2019)

1079 [70] W. Chen, H. Yang, Y. Chen, X. Chen, Y. Fang, H. Chen, Biomass pyrolysis for nitrogen-

1080 containing liquid chemicals and nitrogen-doped carbon materials, Journal of Analytical and

1081 Applied Pyrolysis, 120 (2016) 186-193.

1082 [71] Z. Jin, B. Wang, L. Ma, P. Fu, L. Xie, X. Jiang, W. Jiang, Air pre-oxidation induced high

1083 yield N-doped porous biochar for improving toluene adsorption, Chemical Engineering Journal,

1084 385 (2020) 123843.

1085 [72] W. Yu, F. Lian, G. Cui, Z. Liu, N-doping effectively enhances the adsorption capacity of

1086 biochar for heavy metal ions from aqueous solution, Chemosphere, 193 (2018) 8-16.

1087 [73] F. Lian, G. Cui, Z. Liu, L. Duo, G. Zhang, B. Xing, One-step synthesis of a novel N-doped

1088 microporous biochar derived from crop straws with high dye adsorption capacity, Journal of

1089 environmental management, 176 (2016) 61-68.

1090 [74] Q. Zhou, X. Jiang, X. Li, C.Q. Jia, W. Jiang, Preparation of high-yield N-doped biochar

1091 from nitrogen-containing phosphate and its effective adsorption for toluene, RSC advances, 8

1092 (2018) 30171-30179.

1093 [75] X. Wang, Y. Liu, L. Zhu, Y. Li, K. Wang, K. Qiu, N. Tippayawong, P. Aggarangsi, P.

1094 Reubroycharoen, S. Wang, Biomass derived N-doped biochar as efficient catalyst supports for

1095 CO2 methanation, Journal of CO2 Utilization, 34 (2019b) 733-741.

1096 [76] X. Chen, X. Duan, W.-D. Oh, P.-H. Zhang, C.-T. Guan, Y.-A. Zhu, T.-T. Lim, Insights into

nitrogen and boron-co-doped graphene toward high-performance peroxymonosulfate activation: Maneuverable N-B bonding configurations and oxidation pathways, Applied Catalysis B: Environmental, 253 (2019) 419-432.

[77] J.R.J. Zaeni, J.-W. Lim, Z. Wang, D. Ding, Y.-S. Chua, S.-L. Ng, W.-D. Oh, In situ nitrogen functionalization of biochar via one-pot synthesis for catalytic peroxymonosulfate activation: Characteristics and performance studies, Separation and Purification Technology, 241 (2020) 116702.

[78] Y. Wang, L. Chen, C. Chen, J. Xi, H. Cao, X. Duan, Y. Xie, W. Song, S. Wang, Occurrence of both hydroxyl radical and surface oxidation pathways in N-doped layered nanocarbons for aqueous catalytic ozonation, Applied Catalysis B: Environmental, 254 (2019c) 283-291.

[79] X. Duan, S. Indrawirawan, H. Sun, S. Wang, Effects of nitrogen-, boron-, and phosphorus-doping or codoping on metal-free graphene catalysis, Catalysis Today, 249 (2015c) 184-191.

[80] X. Duan, K. O'Donnell, H. Sun, Y. Wang, S. Wang, Sulfur and Nitrogen Co-Doped Graphene for Metal-Free Catalytic Oxidation Reactions, Small, 11 (2015d) 3036-3044.

[81] J. Liang, Y. Jiao, M. Jaroniec, S.Z. Qiao, Sulfur and Nitrogen Dual-Doped Mesoporous Graphene Electrocatalyst for Oxygen Reduction with Synergistically Enhanced Performance, Angewandte Chemie International Edition, 51 (2012) 11496-11500.

[82] Y. Zhao, L. Yang, S. Chen, X. Wang, Y. Ma, Q. Wu, Y. Jiang, W. Qian, Z. Hu, Can Boron and Nitrogen Co-doping Improve Oxygen Reduction Reaction Activity of Carbon Nanotubes?, Journal of the American Chemical Society, 135 (2013) 1201-1204.

[83] X.-k. Ma, N.-H. Lee, H.-J. Oh, S.-C. Jung, W.-J. Lee, S.-J. Kim, Morphology control of hexagonal boron nitride by a silane coupling agent, Journal of Crystal Growth, 316 (2011) 185-190.

1120   [84] Q. Zhong, Q. Lin, R. Huang, H. Fu, X. Zhang, H. Luo, R. Xiao, Oxidative degradation of

1121   tetracycline using persulfate activated by N and Cu codoped biochar, Chemical Engineering

1122   Journal, 380 (2020) 122608.

1123   [85] M. Sevilla, A.B. Fuertes, The production of carbon materials by hydrothermal

1124   carbonization of cellulose, Carbon, 47 (2009) 2281-2289.

1125   [86] L. Wang, W. Yan, C. He, H. Wen, Z. Cai, Z. Wang, Z. Chen, W. Liu, Microwave-assisted

1126   preparation of nitrogen-doped biochars by ammonium acetate activation for adsorption of acid red

1127   18, Applied Surface Science, 433 (2018a) 222-231.

1128   [87] Z. Wan, Y. Sun, D.C.W. Tsang, Z. Xu, E. Khan, S.-H. Liu, X. Cao, Sustainable impact of

1129   tartaric acid as electron shuttle on hierarchical iron-incorporated biochar, Chemical Engineering

1130   Journal, 395 (2020b) 125138.

1131   [88] X. Xu, Y. Zheng, B. Gao, X. Cao, N-doped biochar synthesized by a facile ball-milling

1132   method for enhanced sorption of CO_2 and reactive red, Chemical Engineering Journal, 368 (2019b)

1133   564-572.

1134   [89] A.P. Mbouopda, E. Acayanka, F.W. Boyom-Tatchemo, G.Y. Kamgang, A.M. Nzeufa, S.

1135   Laminsi, D. Richard, New-route synthesis of N-doped TiO_2 via exposing the $TiCl_3$ precursor to

1136   non-thermal quenched plasma at various times, Materials Chemistry and Physics, 206 (2018) 224-

1137   231.

1138   [90] A. Tiya-Djowe, M.-A. Dourges, J.-L. Bruneel, H. Deleuze, Plasma-deposition of α-FeOOH

1139   particles on biochar using a gliding arc discharge in humid air: a green and sustainable route for

1140   producing oxidation catalysts, RSC Advances, 9 (2019) 4797-4805.

1141   [91] Y. Gao, S. Xu, Q. Yue, S. Ortaboy, B. Gao, Y. Sun, Synthesis and characterization of

1142   heteroatom-enriched biochar from keratin-based and algous-based wastes, Advanced Powder

1143   Technology, 27 (2016) 1280-1286.

1144   [92] L. Xu, C. Wu, P. Liu, X. Bai, X. Du, P. Jin, L. Yang, X. Jin, X. Shi, Y. Wang,

1145   Peroxymonosulfate activation by nitrogen-doped biochar from sawdust for the efficient

1146   degradation of organic pollutants, Chemical Engineering Journal, 387 (2020) 124065.

1147   [93] Y. Sun, I.K.M. Yu, D.C.W. Tsang, X. Cao, D. Lin, L. Wang, N.J.D. Graham, D.S. Alessi,

1148   M. Komárek, Y.S. Ok, Y. Feng, X.-D. Li, Multifunctional iron-biochar composites for the removal

1149   of potentially toxic elements, inherent cations, and hetero-chloride from hydraulic fracturing

1150   wastewater, Environment International, 124 (2019) 521-532.

1151   [94] Y. Sun, S.S. Chen, A.Y.T. Lau, D.C.W. Tsang, S.K. Mohanty, A. Bhatnagar, J. Rinklebe,

1152   K.-Y.A. Lin, Y.S. Ok, Waste-derived compost and biochar amendments for stormwater treatment

1153   in bioretention column: Co-transport of metals and colloids, Journal of hazardous materials, 383

1154   (2020) 121243.

1155   [95] D. Zhong, Y. Jiang, Z. Zhao, L. Wang, J. Chen, S. Ren, Z. Liu, Y. Zhang, D.C.W. Tsang,

1156   J.C. Crittenden, pH Dependence of Arsenic Oxidation by Rice-Husk-Derived Biochar: Roles of

1157   Redox-Active Moieties, Environmental science & technology, 53 (2019a) 9034-9044.

1158   [96] S. Guo, Y. Gao, Y. Wang, Z. Liu, X. Wei, P. Peng, B. Xiao, Y. Yang, Urea/ZnCl2 in situ

1159   hydrothermal carbonization of Camellia sinensis waste to prepare N-doped biochar for heavy

1160   metal removal, Environmental Science and Pollution Research, 26 (2019) 30365-30373.

1161   [97] C. Gai, Y. Guo, N. Peng, T. Liu, Z. Liu, N-Doped biochar derived from co-hydrothermal

1162   carbonization of rice husk and Chlorella pyrenoidosa for enhancing copper ion adsorption, RSC

1163   Advances, 6 (2016) 53713-53722.

1164   [98] F. Yang, L. Sun, W. Xie, Q. Jiang, Y. Gao, W. Zhang, Y. Zhang, Nitrogen-functionalization

1165   biochars derived from wheat straws via molten salt synthesis: An efficient adsorbent for atrazine

removal, Science of The Total Environment, 607-608 (2017) 1391-1399.

[99] Y. Li, B. Xing, X. Wang, K. Wang, L. Zhu, S. Wang, Nitrogen-Doped Hierarchical Porous Biochar Derived from Corn Stalks for Phenol-Enhanced Adsorption, Energy & Fuels, 33 (2019a) 12459-12468.

[100] J. Lu, C. Zhang, J. Wu, Y. Luo, Adsorptive Removal of Bisphenol A Using N-Doped Biochar Made of Ulva prolifera, Water, Air, & Soil Pollution, 228 (2017) 327.

[101] M.V. Nguyen, B.K. Lee, A Novel removal of CO_2 using nitrogen doped biochar beads as a green adsorbent, Process Safety & Environmental Protection, 104 (2016) 490-498.

[102] D. Wang, Y. Sun, D.C.W. Tsang, E. Khan, D.-W. Cho, Y. Zhou, F. Qi, J. Gong, L. Wang, Synergistic utilization of inherent halides and alcohols in hydraulic fracturing wastewater for radical-based treatment: A case study of di-(2-ethylhexyl) phthalate removal, Journal of hazardous materials, 384 (2020) 121321.

[103] X. Duan, Z. Ao, H. Sun, S. Indrawirawan, Y. Wang, J. Kang, F. Liang, J. Zhu, S. Wang, Nitrogen-Doped Graphene for Generation and Evolution of Reactive Radicals by Metal-Free Catalysis, ACS applied materials & interfaces, 7 (2015e) 4169.

[104] Z. Li, Y. Sun, Y. Yang, Y. Han, T. Wang, J. Chen, D.C.W. Tsang, Biochar-supported nanoscale zero-valent iron as an efficient catalyst for organic degradation in groundwater, Journal of hazardous materials, 383 (2020) 121240.

[105] B. Pan, H. Li, D. Lang, B. Xing, Environmentally persistent free radicals: Occurrence, formation mechanisms and implications, Environmental Pollution, 248 (2019) 320-331.

[106] X. Ruan, Y. Sun, W. Du, Y. Tang, Q. Liu, Z. Zhang, W. Doherty, R.L. Frost, G. Qian, D.C.W. Tsang, Formation, characteristics, and applications of environmentally persistent free radicals in biochars: A review, Bioresource technology, 281 (2019) 457-468.

1189 [107] X. Duan, Z. Ao, L. Zhou, H. Sun, G. Wang, S. Wang, Occurrence of radical and nonradical

1190 pathways from carbocatalysts for aqueous and nonaqueous catalytic oxidation, Applied Catalysis

1191 B: Environmental, 188 (2016) 98-105.

1192 [108] X. Duan, H. Sun, K. Jian, Y. Wang, S. Wang, Insights into Heterogeneous Catalysis of

1193 Persulfate Activation on Dimensional-Structured Nanocarbons, Acs Catalysis, 5 (2015f) 4629-

1194 4636.

1195 [109] C. Liu, L. Chen, D. Ding, T. Cai, From rice straw to magnetically recoverable nitrogen

1196 doped biochar: Efficient activation of peroxymonosulfate for the degradation of metolachlor,

1197 Applied Catalysis B: Environmental, 254 (2019b) 312-320.

1198 [110] F. Yao, Q. Yang, M. Yan, X. Li, F. Chen, Y. Zhong, H. Yin, S. Chen, J. Fu, D. Wang, X.

1199 Li, Synergistic adsorption and electrocatalytic reduction of bromate by Pd/N-doped loofah sponge-

1200 derived biochar electrode, Journal of hazardous materials, 386 (2020) 121651.

1201 [111] Y.-X. Liu, S.-M. Du, J. Cao, W.-s. Huang, X.-R. Zhang, B.-P. Qi, S.-H. Zhang,

1202 Simultaneous Determination of Hydroquinone and Catechol by N-doped Porous Biochar-modified

1203 Electrode, Bulletin of the Korean Chemical Society, 41 (2020) 261-265.

1204 [112] M. Wang, Y. Lai, J. Fang, J. Li, F. Qin, K. Zhang, H. Lu, N-doped porous carbon derived

1205 from biomass as an advanced electrocatalyst for aqueous aluminium/air battery, International

1206 Journal of Hydrogen Energy, 40 (2015b) 16230-16237.

1207 [113] Y. Li, L. Liu, R. Shi, S. Yang, C. Zhao, Y. Shi, C. Cao, X. Yan, Natural Okra Shells

1208 Derived Nitrogen-Doped Porous Carbon to Regulate Polysulfides for High-Performance Lithium–

1209 Sulfur Batteries, Energy Technology, 7 (2019b) 1900165.

1210 [114] M. Borghei, N. Laocharoen, E. Kibena-Põldsepp, L.-S. Johansson, J. Campbell, E.

1211 Kauppinen, K. Tammeveski, O.J. Rojas, Porous N,P-doped carbon from coconut shells with high

electrocatalytic activity for oxygen reduction: Alternative to Pt-C for alkaline fuel cells, Applied Catalysis B: Environmental, 204 (2017) 394-402.

[115] K. An, X. Xu, X. Liu, Mo2C-Based Electrocatalyst with Biomass-Derived Sulfur and Nitrogen Co-Doped Carbon as a Matrix for Hydrogen Evolution and Organic Pollutant Removal, ACS Sustainable Chemistry & Engineering, 6 (2018) 1446-1455.

[116] Y. Zhou, Y. Leng, W. Zhou, J. Huang, M. Zhao, J. Zhan, C. Feng, Z. Tang, S. Chen, H. Liu, Sulfur and nitrogen self-doped carbon nanosheets derived from peanut root nodules as high-efficiency non-metal electrocatalyst for hydrogen evolution reaction, Nano Energy, 16 (2015) 357-366.

[117] X. Liu, Y. Zhou, W. Zhou, L. Li, S. Huang, S. Chen, Biomass-derived nitrogen self-doped porous carbon as effective metal-free catalysts for oxygen reduction reaction, Nanoscale, 7 (2015a) 6136-6142.

[118] P. Chen, L.-K. Wang, G. Wang, M.-R. Gao, J. Ge, W.-J. Yuan, Y.-H. Shen, A.-J. Xie, S.-H. Yu, Nitrogen-doped nanoporous carbon nanosheets derived from plant biomass: an efficient catalyst for oxygen reduction reaction, Energy & Environmental Science, 7 (2014) 4095-4103.

[119] F. Liu, H. Peng, C. You, Z. Fu, P. Huang, H. Song, S. Liao, High-Performance Doped Carbon Catalyst Derived from Nori Biomass with Melamine Promoter, Electrochimica Acta, 138 (2014) 353-359.

[120] F. Pan, Z. Cao, Q. Zhao, H. Liang, J. Zhang, Nitrogen-doped porous carbon nanosheets made from biomass as highly active electrocatalyst for oxygen reduction reaction, Journal of Power Sources, 272 (2014) 8-15.

[121] L. Pi, R. Jiang, W. Cai, L. Wang, Y. Wang, J. Cai, X. Mao, Bionic Preparation of CeO2-Encapsulated Nitrogen Self-Doped Biochars for Highly Efficient Oxygen Reduction, ACS applied

54

1235 materials & interfaces, 12 (2020) 3642-3653.

1236 [122] M. Zhang, X. Jin, L. Wang, M. Sun, Y. Tang, Y. Chen, Y. Sun, X. Yang, P. Wan,

1237 Improving biomass-derived carbon by activation with nitrogen and cobalt for supercapacitors and

1238 oxygen reduction reaction, Applied Surface Science, 411 (2017) 251-260.

1239 [123] W.-J. Liu, H. Jiang, H.-Q. Yu, Emerging applications of biochar-based materials for

1240 energy storage and conversion, Energy & Environmental Science, 12 (2019c) 1751-1779.

1241 [124] G. Wang, Y. Deng, J. Yu, L. Zheng, L. Du, H. Song, S. Liao, From Chlorella to Nestlike

1242 Framework Constructed with Doped Carbon Nanotubes: A Biomass-Derived, High-Performance,

1243 Bifunctional Oxygen Reduction/Evolution Catalyst, ACS applied materials & interfaces, 9 (2017)

1244 32168-32178.

1245 [125] K. Wang, S. Zhang, Z. Chen, R. Bao, Interactive effect of electrode potential on pollutants

1246 conversion in denitrifying sulfide removal microbial fuel cells, Chemical Engineering Journal, 339

1247 (2018b) 442-449.

1248 [126] T. Huggins, H. Wang, J. Kearns, P. Jenkins, Z.J. Ren, Biochar as a sustainable electrode

1249 material for electricity production in microbial fuel cells, Bioresource technology, 157 (2014) 114-

1250 119.

1251 [127] K. Zhong, M. Li, Y. Yang, H. Zhang, B. Zhang, J. Tang, J. Yan, M. Su, Z. Yang, Nitrogen-

1252 doped biochar derived from watermelon rind as oxygen reduction catalyst in air cathode microbial

1253 fuel cells, Applied Energy, 242 (2019b) 516-525.

1254 [128] T.M. Huggins, J.J. Pietron, H. Wang, Z.J. Ren, J.C. Biffinger, Graphitic biochar as a

1255 cathode electrocatalyst support for microbial fuel cells, Bioresource technology, 195 (2015) 147-

1256 153.

1257 [129] G. Yue, K. Meng, Q. Liu, One-Step Synthesis of N-Doped Carbon and Its Application as

a Cost-Efficient Catalyst for the Oxygen Reduction Reaction in Microbial Fuel Cells, ChemPlusChem, 80 (2015) 1133-1138.

[130] Q. Liu, Y. Zhou, S. Chen, Z. Wang, H. Hou, F. Zhao, Cellulose-derived nitrogen and phosphorus dual-doped carbon as high performance oxygen reduction catalyst in microbial fuel cell, Journal of Power Sources, 273 (2015b) 1189-1193.

[131] L. Klüpfel, M. Keiluweit, M. Kleber, M. Sander, Redox Properties of Plant Biomass-Derived Black Carbon (Biochar), Environmental science & technology, 48 (2014) 5601-5611.

[132] T. Sun, B.D.A. Levin, J.J.L. Guzman, A. Enders, D.A. Muller, L.T. Angenent, J. Lehmann, Rapid electron transfer by the carbon matrix in natural pyrogenic carbon, Nature Communications, 8 (2017) 14873.

[133] J.R. Miller, P. Simon, Electrochemical Capacitors for Energy Management, Science, 321 (2008) 651.

[134] M. Biswal, A. Banerjee, M. Deo, S. Ogale, From dead leaves to high energy density supercapacitors, Energy & Environmental Science, 6 (2013) 1249-1259.

[135] Z. Li, L. Zhang, B.S. Amirkhiz, X. Tan, Z. Xu, H. Wang, B.C. Olsen, C.M.B. Holt, D. Mitlin, Carbonized Chicken Eggshell Membranes with 3D Architectures as High-Performance Electrode Materials for Supercapacitors, Advanced Energy Materials, 2 (2012) 431-437.

[136] J. Liu, Y. Deng, X. Li, L. Wang, Promising Nitrogen-Rich Porous Carbons Derived from One-Step Calcium Chloride Activation of Biomass-Based Waste for High Performance Supercapacitors, ACS Sustainable Chemistry & Engineering, 4 (2016) 177-187.

[137] D. Hulicova-Jurcakova, M. Seredych, G.Q. Lu, T.J. Bandosz, Combined Effect of Nitrogen- and Oxygen-Containing Functional Groups of Microporous Activated Carbon on its Electrochemical Performance in Supercapacitors, Advanced Functional Materials, 19 (2009) 438-

1281   447.

1282   [138] Y.-H. Lee, K.-H. Chang, C.-C. Hu, Differentiate the pseudocapacitance and double-layer

1283   capacitance contributions for nitrogen-doped reduced graphene oxide in acidic and alkaline

1284   electrolytes, Journal of Power Sources, 227 (2013) 300-308.

1285   [139] L. Wang, X. Li, J. Ma, Q. Wu, X. Duan, Non-activated, N, S-co-doped biochar derived

1286   from banana with superior capacitive properties, Sustainable Energy, 2 (2014) 39-43.

1287   [140] L. Cao, I.K.M. Yu, D.-W. Cho, D. Wang, D.C.W. Tsang, S. Zhang, S. Ding, L. Wang,

1288   Y.S. Ok, Microwave-assisted low-temperature hydrothermal treatment of red seaweed (Gracilaria

1289   lemaneiformis) for production of levulinic acid and algae hydrochar, Bioresource technology, 273

1290   (2019) 251-258.

1291   [141] I.K.M. Yu, D.C.W. Tsang, A.C.K. Yip, S.S. Chen, Y.S. Ok, C.S. Poon, Valorization of

1292   food waste into hydroxymethylfurfural: Dual role of metal ions in successive conversion steps,

1293   Bioresource technology, 219 (2016) 338-347.

1294   [142] J.B. Binder, A.V. Cefali, J.J. Blank, R.T. Raines, Mechanistic insights on the conversion

1295   of sugars into 5-hydroxymethylfurfural, Energy & Environmental Science, 3 (2010) 765-771.

1296   [143] I.K.M. Yu, X. Xiong, D.C.W. Tsang, L. Wang, A.J. Hunt, H. Song, J. Shang, Y.S. Ok,

1297   C.S. Poon, Aluminium-biochar composites as sustainable heterogeneous catalysts for glucose

1298   isomerisation in a biorefinery, Green Chemistry, 21 (2019b) 1267-1281.

1299   [144] S.S. Chen, I.K.M. Yu, D.-W. Cho, H. Song, D.C.W. Tsang, J.-P. Tessonnier, Y.S. Ok,

1300   C.S. Poon, Selective Glucose Isomerization to Fructose via a Nitrogen-doped Solid Base Catalyst

1301   Derived from Spent Coffee Grounds, ACS Sustainable Chemistry & Engineering, 6 (2018b)

1302   16113-16120.

1303   [145] J.A.H. Dreyer, P. Li, L. Zhang, G.K. Beh, R. Zhang, P.H.L. Sit, W.Y. Teoh, Influence of

the oxide support reducibility on the CO2 methanation over Ru-based catalysts, Applied Catalysis B: Environmental, 219 (2017) 715-726.

[146] L. Roldán, Y. Marco, E. García-Bordejé, Origin of the Excellent Performance of Ru on Nitrogen-Doped Carbon Nanofibers for CO2 Hydrogenation to CH4, ChemSusChem, 10 (2017) 1139-1144.

[147] W. Zhang, Y. Li, X. Fan, F. Zhang, G. Zhang, Y.-A. Zhu, W. Peng, S. Wang, X. Duan, Synergy of nitrogen doping and structural defects on hierarchically porous carbons toward catalytic oxidation via a non-radical pathway, Carbon, 155 (2019) 268-278.

[148] T.C. Nagaiah, S. Kundu, M. Bron, M. Muhler, W. Schuhmann, Nitrogen-doped carbon nanotubes as a cathode catalyst for the oxygen reduction reaction in alkaline medium, Electrochemistry Communications, 12 (2010) 338-341.

[149] H.-S. Oh, J.-G. Oh, W.H. Lee, H.-J. Kim, H. Kim, The influence of the structural properties of carbon on the oxygen reduction reaction of nitrogen modified carbon based catalysts, International Journal of Hydrogen Energy, 36 (2011) 8181-8186.

[150] X. Duan, W. Li, Z. Ao, J. Kang, W. Tian, H. Zhang, S.-H. Ho, H. Sun, S. Wang, Origins of boron catalysis in peroxymonosulfate activation and advanced oxidation, Journal of Materials Chemistry A, 7 (2019) 23904-23913.

[151] P. Hu, H. Su, Z. Chen, C. Yu, Q. Li, B. Zhou, P.J.J. Alvarez, M. Long, Selective Degradation of Organic Pollutants Using an Efficient Metal-free Catalyst Derived from Carbonized Polypyrrole via Peroxymonosulfate Activation, Environmental science & technology, 51 (2017) acs.est.7b03014.

[152] W. Tian, H. Zhang, X. Duan, H. Sun, M.O. Tade, H.M. Ang, S. Wang, Nitrogen- and Sulfur-Codoped Hierarchically Porous Carbon for Adsorptive and Oxidative Removal of

1327   Pharmaceutical Contaminants, ACS applied materials & interfaces, 8 (2016) 7184-7193.

1328